Tom Chudley
Scott Polar Research Institute
University of Cambridge
Lensfield Road
Cambridge CB2 1ER
United Kingdom

Tel: +44 (0) 1223 336574
Email: trc33@cam.ac.uk

Scott
Polar
Research
Institute

20th February 2019

Dear Dr Karlsson,

**RE: Response to Referee Comments**

We have received two reviews to our manuscript tc-2018-256 *High accuracy UAV photogrammetry of ice sheet dynamics with no ground control*, both of which were generally supportive of our work and the relevance of the discussed method to the community.

We have adapted the manuscript in light of their constructive comments, for which we are grateful. In addition, we have made very minor textual changes to the manuscript that were not directly requested by reviewers, in order to improve the clarity of the manuscript in light of the reviewer recommendations, or to fix minor errors in the text.

In our responses below, referee comments are shown in italicised **blue**, our response in **black** and changes in manuscript in **red**. We have also attached a revised manuscript with highlighted changes: page numbers in the text below refer to this highlighted version of the manuscript.

Thank you for your consideration of our revised manuscript, which we hope is now acceptable for publication. Please continue to address further correspondence to me at trc33@cam.ac.uk.

Sincerely,

Tom Chudley and Co-authors

**Comments by Reviewer #1, Guillaume Jouvet, and responses:**

*Unmanned Aerial Vehicles (UAV) photogrammetry has become a very valuable tool to generate high-resolution ortho-images and Digital Elevation Models (DEMs) for geoscientific studies at relative low cost. UAV are of special interest in glaciology, as UAVs can survey remote and hardly accessible glaciers. Repeat UAV surveying, SfM-MVS photogrammetry together with feature-tracking method can be used to track changes of the glacial terrain over time, as for instance due to ice flow motion, melt or calving. However, the inter-comparison of UAV-based photogrammetrical products requires very accurate geo-referencing. So far, it was mandatory to install Ground Control Points (GCPs) next to zones of interest to obtain a sufficient level of accuracy. This need of GCPs was therefore the Achille heel of UAV photogrammetry for glacier surveying as it is difficult to install a network GCPs in such an extreme environments. Direct georeferencing (not based on GCPs, but on camera locations) is key to overcome this issue, but this requires (at least) accurate geotagging of aerial pictures – a level of precision that can not be achieved by standard GPS (SPS).*

*This study solves this issue by the means of miniature, low-cost and cm-accurate differential GPS inboard the UAV. The added-value of this technique is illustrated by the first-ever velocity field derived by UAV of the interior of an ice sheet (i.e. without any immobile margin serving as reference, and without using any GCPs).*

*This is an important contribution as it introduces a promising and affordable technology for the surveying of glaciers, and their changes over time, with significant improvements compared to former methods. Beside this, the paper contains a lot of technical details that are necessary for replication. I have one major comment (see below) about the uncertainty assessment – which is a central question in this paper. I also have others specific and minor comments that might help to improve the paper.*

We are grateful to Dr Jouvet for his helpful and supportive review. Below, we show how we have revised the manuscript in light of his comments and recommendations.

**Major comment**

*My main concern is about the uncertainty assessment in the horizontal direction. The authors claim that they get a 0.07 m horizontal accuracy. However, this number is based on the assumption that feature-tracking error contributes by 0.5 pixel of the uncertainty. It means that 0.07 is obtained by subtracting 0.10 (or estimated feature tracking error) to 0.17 of RMSE. Is it not a bit shortcoming? Assume the feature-tracking performs better than 0.5, it means that the uncertainty your are trying to estimate is larger. From your results, we can reasonably say from your result that 0.17 is the combined uncertainty of the two possible sources of error – this is already a very strong result! Yet, if one wants to clearly evaluate the contribution of each, this can only be done separately. For Feature-tracking (or template matching), this might be difficult. Yet for SfM photogrammetry only, have you tried to perform surveys of an accessible terrain with GCPs for error assessment? This can be done anywhere, not necessarily in Greenland.*

And also specific comment: *Section 2.5 As said before, I think it is dangerous to subtract an unknown error on the featuretracking to sRMSE. I'd simply use sRMSE as an upper bound, mentioning that this estimate might be sub-optimal as it might contain a contribution external to SfM.*

We agree with this assessment. Whilst 0.5 pixels is a typical value to apply for feature-tracking uncertainty, it is likely not equally transferable to this use case. Instead, we have chosen to ignore feature tracking error and estimate an upper bound for the horizontal uncertainty as follows:

$$S_{RMSE} = \sqrt{\sigma_{xy}^2 + \sigma_{xy}^2}$$

This provides a value of 0.12 cm (1.1 GSD), which we clarify in-text includes feature-tracking error and is likely an upper limit (this is supported by comparisons to alternative studies, which normally have a horizontal error 0.5-1.0 GSD).

We have changed (i) the methods (P8L17-28), (ii) relevant references throughout the text to horizontal uncertainty (P1L10-11, P12L11, P16L4-5, P20L5-6), and (iii) added text in the discussion clarifying the inclusion of feature tracking error when comparing to other papers that have estimated GNSS-AT error (P16L8-10) (see below).

**Specific comments**

*What about giving the uncertainty in pixel rather than in meter (here you have sub-pixel accuracy)? If you were flying twice higher with twice more spaced lines, would you get the same sub-pixel accuracy (but the pixel would be twice bigger)? If yes, your result given in pixel would be more general. Of course, this only if the accuracy scales with the resolution (or equivalently the flight altitude).*

It is important that we deal with uncertainties in metres and not only in pixels as consideration of uncertainty in velocity is ultimately dependent on displacement uncertainty in metres. However, we agree that the it would be useful to present relative pixel uncertainties, not least because it would place our absolute uncertainties into context (decimetres cf. centimetres in other studies due to varying flight altitudes). We choose to present this not as pixels but as units of ground sampling distance (GSD), which is the generalised unit used in other studies. We have referred to this new uncertainty (~1.1 GSD in the horizontal and ~1.3 GSD in the vertical) alongside absolute values throughout the paper (P1L10-11, P12L11, P16L4-5, P20L5-6). Further, this value allows comparison with alternative non-glaciological studies, which does show that relative uncertainty is broadly the same (i.e. scales with altitude) once normalised against GSD - see further discussion below.

*Additionally, you do not provide any estimate of the inaccuracy of Emlid Reach of the camera location (about 1 cm horizontally and vertically from my experience, not millimeter). Does the final inaccuracy of the DEM and orthophoto partly result from this small-but-existing error of the camera location or other uncertainties in the SfM-MVS (lens calibration, ...)? If both, can you quantity the contribution of each? This is related to my previous point: if the small but existing inaccuracy of the position given by Emlid Reach receiver plays no role (because it is overridden by other sources of errors), then the final accuracy of the SfM might broadly scales with the resolution (GSD). In that case, I think the result inaccuracy is better given in pixel.*

Regarding Emlid Reach uncertainty: RTKLIB output reports standard deviations of ~0.6 mm horizontally and ~1.1 mm vertically for fixed solution data. Given the final estimated uncertainty of the order of a decimetre, we assume the Emlid Reach uncertainty is subsumed into other uncertainties - largely that of the

photogrammetry itself, that of lens calibration error, etc., that exist in the 'black box' of Photoscan. However, we don't feel in a position to quantify this, and cannot find any examples of this being done in previous papers utilising GNSS-AT, which also present a single 'cumulative' error estimate. With regards to your last point, It is worth pointing out, given the above, that this might *not* be the case at lower elevation, where ~1cm GPS error is a significant component of the 2-3cm final error.

We have explicitly included final reported GPS uncertainty in the methods section 2.3:

P7L25: RTKLIB camera location outputs are estimated to have standard deviations ~0.6 mm horizontally and ~1.1 mm vertically for fixed solution data.

*It would be good to add non-glaciological references in the discussion, e.g. studies that assess the accuracy of PPK UAV SfM photogrammetry. Of course, the results always depend on many settings that depend on the UAV equipment and type of mission flown (altitude, overlap, ...). Yet, numbers of recently release commercial products (Sensefly, Wingtra, ...) equipped with similar technology offer sub-pixel accuracy. How does your result uncertainty compare with other non-glaciological studies applying SfM UAV photogrammetry and GNSS-AT?*

Thank you for this recommendation - it has proven particularly useful as a point of comparison. We have taken note of various reported accuracies (our estimated errors match well with previous estimates) and included them as points of comparison in the discussion:

P16L5-16: With well-constrained geolocation, horizontal (vertical) accuracies can be as high as 0.5-1.0 GSD (1.5-2.0 GSD) (Benassi *et al.* 2017). Our estimated accuracies are very close to these theoretical values -- in fact, our vertical accuracy is even higher. Our lower accuracy in the horizontal is likely due to the fact that $s_{RMSE}$ Includes feature tracking error. Common estimates of the latter can be up to 0.5 pixels (e.g. Quincey et al., 2015), which if assumed in our use case would bring the $\sigma_{xy}$ estimate down as little as ~0.5 GSD. Our estimated accuracy values agree well with previously reported GNSS-AT derived estimates. For instance, Fazelli *et al.* (2016) report horizontal (vertical) accuracies of 0.6 (1.0) GSD using a low-cost customised multirotor UAV. Our accuracies also align with reported horizontal (vertical) accuracies of commercial fixed-wing drones, which offer similar performance to our low-cost alternative at a considerably higher price. Studies using the eBee RTK have reported horizontal (vertical) accuracies of 1.0 (1.2) GSD (Roze *et al.* 2014), and 0.6-1.2 (0.8-4.0) GSD (Benassi *et al.* 2017), and 0.8 (1.8) GSD (van der Sluijs *et al.* 2018), whilst the WingtraOne PPK has reported horizontal (vertical) accuracies of 1.3 (2.3) GSD (Ng and Buchheim, 2018).

Furthermore, we have expanded our range of methodological references in the introduction (we have outlined this fully in a response to similar comment by reviewer #2).

*It would be interesting to deepen the gain of performing multi-level flights and quantify the reduction of the bowling effect (l 22-26 p 4), e.g. by performing the SfM photogrammetry twice i) once with one flight level ii) once with two levels, and differentiate the 2 DEMs.*

And also minor comment: *l 18-20 p 15 It would be interesting to quantify the reduction of the bowing effect.*

In these two comments, it is suggested that it would be interested to quantify the impact of (i) oblique imagery and (ii) GNSS-AT on the established warping effect visible in non-optimal SfM surveys. Whilst we agree it would be interesting to quantify the impact, given: (i) the scope of the study; (ii) the lack of a control dataset e.g. from terrestrial laser scanning; and (iii) our relative expertise, we do not think we would be able to add anything meaningful to the literature. This topic has been given a comprehensive treatment by Mike James and colleagues in their relevant papers (James and Robson, 2014, and James *et al.* 2017 - in particular see fig. 6 of the latter) and are referenced in the text at appropriate points. However, since this work has been in discussion, another excellent detailed assessment of the impact of oblique imagery has been published by Nesbit and Hugenholtz (2019), which also makes specific practical recommendations as to the when and how of incorporation of oblique imagery into flight routines. We have added reference to this in the text (P5L10). Given that we may be the first to incorporate this recommendation in the glaciological literature, we hope these detailed assessments will provide other researchers with enough information to be able to put these techniques - particularly the relatively simple oblique image capture - into wider practice.

*I find the calving event you captured (l 26-30 p 8) very interesting, especially because you get a clear discontinuity in the velocity field indicating that a large iceberg is about to collapse. There is interesting material for discussion (influence of the plume, can this crevasses be propagating by hydro-fracturing, or similarity with the proceeding reported in (Jouvet, 2017, TC)?). However, your text is mostly factual, and does not discuss at all what processes might be responsible for these observations. Discussing these observations (in the discussion) and making a parallel with similar ones reported in the literature would be a true added-value.*

We agree that the calving event shown in the results is interesting. However, we consider that detailed analysis and discussion of the event (along with the others observed across the study period) belong as part of their own study - the event shown here is simple a case study to highlight a potential use case of the method. Nevertheless, considering that even the limited data shown here may be of interest to others working on calving dynamics, we have included additional information in the relevant results section, including quantifications of crevasse width, depth, and calving volume (P9L30-P12L5). We have added an additional range of subfigures to Figure 5 (d--f) showing DEMs that are helpful to visualise crevasse formation, and have changed the calving cross-section shown in Figure 4b so it matches that of the calving event in Figure 5, in order to improve the flow and cohesion of the results.

*It would be more logical to move section 4.3 (Future direction) after the conclusion.*

We have retained section 4.3 as it was, as we prefer to finish the manuscript with the conclusions.

**Minor Comments**

*l 15 p 2 "0.09 m per m–1" should be "0.09 m per m"?*

Corrected.

*l 35 p 2 "Here, we show that ... is used to geolocate imagery acquired over a large Greenlandic outlet glacier with a fixed-wing UAV." You could keep this statement more general (removing "Greenlandic outlet" and "fixed-wing") as your method is inherent to Greenland and type of UAV.*

Rewriting of this paragraph in response to comments by Reviewer #2 has resulted in the removal of this sentence.

*l 8 p 4 1 Kg looks overestimated for a Sonny alpha 6000 unless the lens is really heavy?*

Agreed - 1 kg refers to our estimate of the maximum potential payload given our configuration. The true scientific payload weight (including camera, trigger, L1 GPS, antenna, and ground plane) is approx. 500 g. Rewritten (P4L20-21).

*l 8 p 4 1500 $ sounds quiet low (my owns cost more than twice when summing the costs of all components). Does it include only the cost of the frame only? and anything else you need to fly it (RC, Second Elmid Reach, ...).*

NB that we refer to the cost in GBP, not USD, so the true value is closer to USD 2000 - although this does not account fully for the difference in our estimates.

We have referred back to our components list and re-checked prices and can confirm that this this is an accurate estimate for the set up of a complete standalone unit including Skywalker frame, PixHawk autopilot (and supporting hardware), flight hardware (LiPos, ESC, motor, servos, props etc.), and scientific hardware (camera, GPS, and supporting hardware). However, it does not include the ground components (Tx and LiPo charger, which came to ~GBP 300), nor the Trimble GPS ground equipment, which, as discussed in section 4.3, is of considerably higher cost, albeit often a common pre-existing part of glaciological field campaigns.

Given the above, we hope that the discrepancy is less than originally considered, and to within the bounds of reasonable error given individual hardware choices, pricing variations, and recent currency fluctuations. We have altered the text to clarify the cost refers to a single complete flight unit:

P4L25-28: The cost of a complete flight unit (including frame, hardware, and scientific payload) was approximately ~ £1500 per unit. Further necessary ground equipment, which could be shared between units, came to ~£300: this includes the radio transmitter and lithium polymer battery charger, but not the ground-based GPS (sections 2.3, 4.3).

*l 14 p 4 "Artupilot's Mission Panner": I would remove "Artupilot's"*

In the interests of describing a complete and detailed workflow, we feel it is important to refer at least once to the exact software used - particularly as this software is not synonymous with (albeit closely associated to) Arduplane firmware.

*l 18 p 4 GSD of ~ 11 cm*

Corrected.


*l 18 p 4 "Out camera" should be "Our camera"*

Corrected.


*l 20 p 4 Did you process raw images in PhotoScan? or JPEG. I understand you processed raw otherwise why recording them in raw? If not, please, clarify.*

We chose to record in RAW to avoid the potential influence of processing lossy file formats such as JPEG. Photoscan cannot process RAW images, but were converted to 16-bit Tiff format for AgiSoft (see also Ryan *et al.* 2017). We have clarified the sentence as follows:

P5L2-3: Photos were recorded in RAW format to ensure lossless storage of images, and converted into Photoscan-compatible 16-bit tiffs before processing.


*l 10-12 p 5 "... equivalent to 2-3 mm" I'm not sure to understand these numbers. Do they refer to measure of the carrier phase? the accuracy? Maybe this sentence could be a bit more explained for novices in GNSS systems.*

We have rewritten the sentence for greater clarity:

P5L27-29: Higher positioning accuracy than is offered by the SPS can be achieved by using differential carrier phase positioning, which makes use of the ability of GNSS receivers to measure the carrier phase to one hundredth of a cycle, equivalent to about 2 mm in distance (Leick *et al.* 2004)


*l 15-20 p 6 The unnecessary usage of RTK can be summarized more efficiently in a single sentence: "Whilst the Emlid Reach GNSS receiver is capable of RTK, we used instead PPK positioning for simplicity as the RTK brings additional technical constrains and is not more accurate than PPK"*

In an effort to balance this recommendation against a recommended addition from reviewer #2, we have rewritten the paragraph as follows.

P7L1-8: Whilst the Emlid Reach GNSS receiver is capable of real-time kinematic (RTK) we used instead post-processed kinematic (PPK) positioning for three primary reasons. First, PPK does not rely on maintaining a reliable real-time radio link with a GNSS base station, which would introduce additional technical constraints. Second, PPK solutions are also often more accurate than RTK solutions as precise ephemeris data for the GNSS satellites is available during post processing. Third, absolute positioning using

RTK requires a stationary reference station with a known position, which is not possible in real time on an advecting ice surface.

Above, we simplify part of the explanation, but choose to keep the additional clarification about absolute positioning using RTK, which is an additional constraint for operating on ice sheets that some readers may not be concerned with (and hence decide that RTK is viable).

*l 9 p 7 DEMs always have coarser resolution than ortho-images after being produced by SfM-MSV. If you have GSD of 11 cm, 15 cm is logical resolution to output orthoimage. However, is 20 cm optimal for the DEM? Do you really get that resolution?*

An optimal DEM resolution is recommended by Photoscan: given the proprietary / black box nature of Photoscan it is hard to assess the exact nature of this recommendation, but it is apparently based on the effective point cloud resolution (which scales with quality of reconstruction), with some additional leeway provided to avoid interpolation. We were consistently recommended a resolution of ~18 cm across point clouds, so chose 20 cm as a coarser option to accommodate some further variation. We have added the following qualifier in the text:

P8L2: ... based on recommended output resolutions from Photoscan.

*l 16 p 8 I can see crevasses on Fig 4b, but I can not really observe crevasse opening (i.e. positive strain rate) on this figure. Either reconsider the figure or rephrase.*

Tto provide an alternative example, we have replaced the transect in Figure 4b  with another (see updated Fig. 1a) where crevasse opening is clearly visible. This new transect covers the same calving event shown in Figure 5, and hence provides additional cohesion through the section. We have also referenced new subfigures 5d--e, where the opening of this crevasse in plane view is clearly visible in the DEMs of figure 5d and 5e.

*l 20 p 8 Fig. 3c, 4a and 5*

We have added references to these figures.

*l 22 p 8 "Our method is sensitive to small changes occurring at the calving front": I don't understand this sentence. Is the method or the calving front sensitive to small change?*

The method. We have rewritten as follows to clarify:

P7L22-23: Our method is sensitive to relatively small dynamic changes at the calving front

*Fig 4, caption A large-scale calving event occurs between ... of July.*

We have added 'large-scale' to the description.

*l 14 p 11 "track displacement of <1m" would be better given in pixel.*

Changed to < 5 pixels.

*l 4-6 p 13 This sentence seems redundant with one sentence of the section before. Maybe this is a way to avoid this redundancy.*

Changed as follows:

<span style="color:red">P14 L1-2: We can test the robustness of the inland surveys by comparing contemporaneous velocity fields from independent flights.</span>

*Fig 9, caption Specify along what profile these velocity fields were taken.*

Thanks for highlighting this absence. Transect F9 has been added to fig. 1c. The caption has been edited to reflect this.

*l 13-15 p 14 It might be good to add that it worked as water of supra-glacial lake was clear/transparent. Of course, this would not work with turbid water (unlikely to be met on supra-glacial lake).*

Agreed. Changed as follows:

<span style="color:red">P15L6-7: ...is sufficient to measure horizontal displacement through (non-turbid) water such as supraglacial lakes.</span>

*l 16-19 p 15 "radial error", radial with respect to what? the lens? "can be reduced significantly with the introduction of accurate aerial georeferencing (James et al., 2017)" ⇒ "can be reduced significantly with the introduction of GNSS-AT (James et al., 2017)" if this is the case, better use always the same terminology for clarity.*

Yes, the lens. Sentence rewritten as follows:

<span style="color:red">P17L3-6: ...likely a 'bowing' effect from radial lens distortion error in the fixed or self-calibrated camera calibration (James and Robson, 2014), a feature that can be reduced significantly with the introduction of precise georeferencing (James et al., 2017).</span>

*l 22 p 15 We actually had more than 2 GCPs on each side, but instead about 10 GCPs on each side, plus a few moving with the ice.*

8

Thanks for clarification. We have corrected the GCP counts in the text (P17L9).

*Fig 2b is too small, would require either more explanations or can be removed as well as the chain of GPS is sufficiently well explained in the text.*

We consider figure 2b to be a useful visual aid to support description in the text so have chosen not to remove it - however, we have altered and enlarged the subfigure to better fit the aspect ratio provided by figure 2.

*Fig 10, caption split last word 'lakebed'*

Corrected.

*l 15 p 16 high-resolution in-situ GNSS measurements*

Corrected.

*l 5 p 17 "had negated cross-correlation 10" ???*

Corrected (and clarified).

P18L16: ...where changes in the supraglacial hydrological network disrupted feature tracking (Fig. 10).

*l 7 p 17 velocity variation due to lake drainage or precipitation events are not necessarily expected right under the supraglacial lake, but could occur far away (dependent on the un/efficiency of the subglacial hydrological system). I'm wondering whether there is a confusion between 2 different things: i) mapping of supraglacial lake (which might be useful to track possible drainage) ii) consequence of lake drainage on the ice velocity. But the two are most likely not to be observed in the same region.*

Supraglacial lake drainage results in local accelerations in ice velocity that have previously been observed with in-situ GNSS measurements (Doyle *et al.* 2013, among others). UAV-derived data would be able to show both the geomorphological changes referred to in point (i) and the impacts on ice velocity referred to in point (ii). We have real examples of both from our 2018 field season - this will be published at a later date.

*l 21 p 17 Is full DSO geolocation already available at affordable price, or very expensive, or still in research development? What gain would be expected using full DSO (compared to GNSS-AT)? Could you add this information?*

DSO is well established for aerial photogrammetry, and has been proven for UAV applications (see Cucci *et al.* 2017, which is also cited in-text). However, we are not aware of any applied geoscience that utilises full DSO. Speculating, this may be because 'we' (geoscience teams looking to apply existing, if novel, methods

rather than develop new ones) are already familiar with GPS post-processing from other field applications, and are more comfortable with applying this in UAV scenarios. With regards to potential pricing, the Piksi Multi (the $1000 dual-frequency example) comes with an IMU, and hence should theoretically allow for full ISO, but at the time of writing their white paper appears out-of-date and does not utilise the IMU, instead relying on the IMU in the PixHawk autopilot module, which introduces problems due to the low data quality and temporal matching.

To summarise this digression - we have added the following sentence at the paragraph in question:

<span style="color:red">P19L12-13: However, we are not aware of any applied use of UAV-based DSO in the geosciences at the time of writing.</span>

<span style="color:blue">*l 32-33 p 17 "Firstly, the integration of these systems allows for the realisation of a truly lowcost, GCP-free UAV-MVS workflow for glaciological applications." This sentence looks unnecessary to me (and even somewhat harming your work). If I understand well, the gain of using dual-frequency GNSS receiver (instead of single) is to obtain absolutely accurate locations, and not being constrained by the 10 km max distance separation between rover and base? Therefore, this would relax the constraint of the chain GNSS receiver (to determine the absolute position of the Emlid Reach base station) you implemented for getting accurate absolute georeferencing. I don't think you expect an improved relative geo-location with dual-frequency receiver, and then a reduced uncertainty?*</span>

Thank you for the useful comment. We have rewritten the first two points as follows, which hopefully more clearly highlights the key advantages of (i) cost and (ii) baseline extension.

<span style="color:red">P19L23-30: Firstly, the integration of these low-cost systems would reduce the initial capital cost of projects that do not already have access to an expensive dual-frequency GPS receiver. Second, these GPS receivers are small and light enough to fit on small-sized UAV airframes, and hence allow for (i) an extended flight baseline, and (ii) direct kinematic correction against an off-ice reference station (i.e. the removal of the need for processing the intermediate base station `B1' in ice sheet environments)</span>

<span style="color:blue">*caption, Fig 3 'seperation' should be 'separation'*</span>

Corrected.

## References

Cucci, D. A., Rehak, M., and Skaloud, J. (2017). Bundle adjustment with raw inertial observations in UAV applications, ISPRS Journal of Photogrammetry and Remote Sensing, 130, 1–12.

Doyle, S. H., Hubbard, A. L., Dow, C. F., Jones, G. A., Fitzpatrick, A., Gusmeroli, A., ... & Box, J. E. (2013). Ice tectonic deformation during the rapid in situ drainage of a supraglacial lake on the Greenland Ice Sheet. The Cryosphere, 7(1), 129-140.

James, M. R. and Robson, S. (2014). Mitigating systematic error in topographic models derived from UAV and ground-based image networks, Earth Surface Processes and Landforms, 39, 1413–1420, https://doi.org/10.1002/esp.3609, 2014.

James, M. R., Robson, S., and Smith, M. W. (2017). 3-D uncertainty-based topographic change detection with structure-from-motion photogrammetry: precision maps for ground control and directly georeferenced surveys, Earth Surface Processes and Landforms, 42, 1769–1788,2017.

Ryan, J. C., Hubbard, A., Box, J. E., Brough, S., Cameron, K., Cook, J. M., ... & Irvine-Fynn, T. (2017). Derivation of high spatial resolution albedo from UAV digital imagery: application over the Greenland Ice Sheet. *Frontiers in Earth Science*, *5*, 40.

**Comments by Reviewer #2, Oliver Wigmore, and responses:**

*The manuscript "High accuracy UAV photogrammetry of ice sheet dynamics with no ground control" outlines a method for the collection of high accuracy DEMs and orthomosaics from UAV without the use of GCPs, referred to as GNSS-AT. This method is applied to two study sites (calving face and internal region) on the Store glacier in Greenland. Perhaps the greatest limitation to UAV surveys is the collection of GCPs, this is particularly true for glacier environments where access to the survey area is often impossible. The method outlined by the authors provides a low cost, relatively simple method to solve this problem. It is important to point out that this solution is not especially novel, as it has been implemented relatively widely outside of glaciology. However, this is certainly one of (if not) the first applications of the method to glaciology and is applied over an interesting and challenging environment, providing new insights into these systems. I believe this paper is a unique contribution and will find widespread interest within the glaciologic community, and within the broader earth sciences. The authors do an excellent job of explaining the method in a logical and easy to follow manner. The manuscript is well written and logically laid out.*

We are grateful to Dr Wigmore for his helpful and supportive review. Below, we show how we have revised the manuscript in light of his comments and recommendations.

**Major Comments**

*One issue that is not discussed is the role of UAV pitch, roll and yaw on the accuracy of the camera positions. The authors apply a standard offset of -7.9cm in Y direction and +13.2cm in the Z direction. However, the actual offset between the antenna centre and the camera sensor centre will change as a function of the attitude of the UAV itself. The only way to correct this is to collect accurate IMU measurements of the UAV/Camera attitude at time of image capture. Given the financial constraints of a high quality IMU (which are clearly discussed) this is not possible. But it would be good to include mention of this as a possible error source and to calculate a ballpark estimate of this error. This can be done by looking at the IMU record from the pixhawk to identify the range of pitch/roll/yaw experienced during the flight and then calculating the impact of these values on the offset values. Also, a picture of the UAV setup showing this offset would help. Finally, I presume that the Y offset would flip depending which direction the UAV is flying? Is that the case? And if so how is it accounted for? Best practice for this design and without an IMU is to install the GNSS antenna directly above the camera so that only the Z offset is considered, and this is more or less static given vertical offsets are typically small.*

GPS/INS offset is implemented fully as a feature of Agisoft Photoscan and the reviewers' concerns are fully accounted for. X, Y, and Z here refer to a coordinate system with the point of origin as the camera with flight attitude taken into account (fig. 1). For more information see pages 56-57 of the Photoscan 1.4 User Manual (Agisoft, 2018).
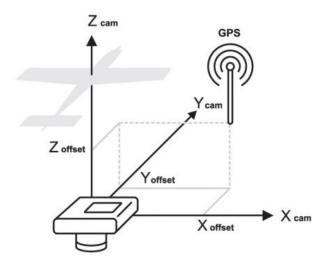
**Figure 1** | *GPS/INS offset coordinate system. Figure taken from Photoscan documentation (Agisoft, 2018).*

We have adjusted the text in the methodology to clarify this coordinate system (P7L32).

*While this technique is relatively new in its application to glaciology, there have been a number of journal publications and grey literature that discuss the benefits and accuracy of GNSS-AT methods. The authors should include some of these citations and briefly mention this work in the introduction and/or discussion. Also some of these papers and industry grey literature compare GNSS-AT methods against more common GCP methods, which is arguably the best way to assess the accuracy of GNSS-AT. This is not done in this paper so would provide strong justification for the viability of the method.*

We agree that our paper is not the first to discuss the benefits of GNSS-AT as applied to UAV-based SfM, and did not intent to inadvertently imply that. The original contribution our paper makes with regards is as follows:

- The first application to glaciology, and one of the very few applications in geoscience generally.
- Implementation of GNSS-AT in a low-cost DIY frame, with a detailed and replicable description of methods.
- A modification of the method to allow for operation of a base unit on an advecting ice surface.
- Validation that the method is useful to assess ice dynamics via feature tracking methods.

On top of the papers we had already cited (Blankenberg, 1992; Hugenholtz *et al.* 2016; Benassi *et al.* 2017), we have incorporated further examples of GNSS-AT photogrammetry methods and accuracy assessment in the introduction (Mian *et al.* 2015, Fazeli *et al.* 2016). Applied use in the geosciences is currently extremely limited, but we have been able to find two examples of geosciences applications of GNSS-AT (in this case, RTK) outside of an accuracy assessment environment (Van der Sluijs *et al.* 2018, Strick *et al.* 2018).

We have also re-emphasised these papers in additional text in the introduction, introducing GNSS-AT firmly in the context of previous work, whilst highlighting the added value our work provides.

P3L1-13: Recent developments in lightweight, low-cost GNSS technology have allowed for the proliferation of a new technique whereby differential carrier-phase GNSS positioning is used to accurately geolocate imagery and subsequent photogrammetric products. This technique, known as GNSS-supported

In addition, we have included white papers by senseFly (Roze *et al.* 2014) and Wingtra (Ng and Buchheim, 2018) in later discussions of comparative GSD-scale uncertainties suggested by reviewer #1, although given their status as grey literature we have elected to not include them in the introduction.

*One final critique is the accuracy assessment. While I believe what was done is acceptable and does prove the method, it would be beneficial to have some sort of external comparison. Either by comparing the GNSS-AT method to the more typical (and accurate) GCP method, or to some other dataset, e.g. terrestrial/airborne LiDAR. This could be done over a small subset area where access is not as much of an issue – e.g. the bedrock zone.*

During our flights at the front, we did actually attempt to record validation GCPs. Here, we replicated the work of Ryan *et al.* (2015) and assessed a number of boulders across the northern side of the calving front visible in UAV orthophotos. Whilst this was adequate for error assessment when using the previous method of geolocation, our method was accurate enough that a the most we could say from this assessment was that our method was better than metre-scale (i.e. sub-boulder) accuracy (fig. 2). Whilst this was a pleasant surprise regarding the unexpected accuracy of the method, it did mean that we had to find alternative ways of estimating uncertainty, taking advantage of the number of repeat flights we made to assess variation rather than absolute error.
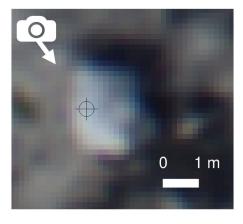


**Figure 2** | *Example of validation GCP collection (left) and comparison against orthophoto (right) at calving front. Direction of photograph origin shown by white marker.*

We strongly agree that in an ideal world we would have access to a validation dataset. However, given the the remote location of the field site, and that our main site was on the ice sheet and not the front, there simply were limitations in what we could and could not achieve with the time available.

**Specific Comments**

*3:4 technically the second 'bedrock' exposure area is feasible to install GCPs, reword this accordingly.*

Reworded as follows:

P3L15 ...settings where on-ice GCPs are not feasible.

*3:5 prohibits should be prohibit*

Corrected

*3:12 at last 1948 should be at least 1948*

Corrected

*3:16 missing units, guessing km – should be "at least 30 km inland"*

Corrected

*4:7 Delete "a" – "the UAV is capable of ~1hour of flight time at ~60km"*

Corrected

*4:16 "allowing flight plans to avoid collision with cliffs" this sentence is awkwardly worded, perhaps rephrase*

Clarified as follows:

P4L32: ...avoiding collision with high relief topography at the glacier margins.

*4:18 "Out camera" should be "Our camera"*

Corrected.

*4:25 Great method! Is there a reason you didn't do this over the calving face as well?*

Thank you! Yes, there is. Our primary concern was one of flight endurance at the calving front (NB. the difference in scale between figs. 3 and 7). We chose to prioritise collecting four complete parallel flight paths of the entire width of the calving front over collecting oblique imagery. We considered that the far more extreme relief in the form of large crevasses and seracs at the front made additional oblique angles less essential than inland, where the surface was relatively flat. Briefly clarified in the text as follows:

P5L6: Flight paths in the ice sheet interior, where flight endurance allowed, also included a lower-altitude ~200 m along-track flightline...

*5:15 Repeats information presented briefly at 4:10 – Perhaps you can remove the text at 4:10 as an expanded discussion is included here.*

We have rewritten the two lines to emphasise hardware and components (former) and data production (latter) in an effort to reduce replication.

P4L21-23To allow for direct georeferencing of each photo location, we included an on-board lightweight L1 carrier-phase GNSS receiver (an Emlid Reach, using a small Tallysman TW4721 antenna with a 100mm ground plane).

P5L30-32: To obtain accurate camera positions we post-processed 5 Hz data logged by the on-board L1 carrier-phase GNSS receiver. Data were post-processed using...

*6:14 "was achievable" do you mean "was located nearby"*

Corrected

*6:14 If you used the EMLID reach in RTK mode you would be using the EMLID as the base station, correct? In which case the base station would only be single frequency. So this is another reason not to use the EMLID in RTK mode I believe. Or can EMLID interpret RTK corrections from other base station receivers (e.g. trimble etc?). On that note, I didn't see the make and model for the local dual frequency base station "B1". Also, reference station is trimble Net R9 receiver, but antenna not provided. Good to include these details if available.*

The Emlid Reach plays nicely with the open-source RTKLIB, so it should theoretically be possible (albeit probably finicky) to combine different hardware to achieve RTK results. But you would still need to know the base station position in real time to achieve absolute RTK positioning.

The base station (B1) and reference (B2) stations are as follows: we have clarified these in text.

- BASE - Trimble R9s receiver - Zephyr 3 Antenna
- REFERENCE -  Trimble NetR9 receiver - Zephyr 3 Geodetic Antenna

P6L9-11: Clarified base and reference station models + antennas in text.

*6:15 PPK solutions are also often more accurate than RTK solutions as precise ephemeris data for the GNSS satellites is available during post processing.*

Thank you for highlighting this point - we have added it to the paragraph and rearranged it into a numbered list to make it comprehensible:

P7L3-6 ...we used instead post-processed kinematic (PPK) positioning for three primary reasons. … Second, PPK solutions are also often more accurate than RTK solutions as precise ephemeris data for the GNSS satellites is available during post processing.

*8:20 detected over "a" six-hour period*

Corrected.

*8:27 More "than" 48 hours. . ..*

Corrected.

*11:5 reveals, perhaps reveal?*

Corrected.

*12:1 Couldn't you install the on ice base station for a few days (anywhere on the ice) and then process that data using the NRCAN PPP kinematic processing method (or OPUS) and then just pull the position of the base station at the time of the flight and use that as the static position for PPK processing of the UAV. That would mean you could work anywhere on the ice sheet and wouldn't be constrained to the 60km distance from the static reference station installed on bedrock.*

The reference to a ~60 km limit at this point in the text refers not to the reasonable baseline of dual-frequency processing but on the limit of reliable feature tracking given the observational errors in feature tracking versus daily glacier displacement.

Regardless, it is true to an extent that the base station could alternatively be positioned using kinematic PPP. However, whilst it is the case that PPP can achieve centimetre-level positioning given 24 hours of static observations (King *et al.* 2002), a fast-flowing glacier surface is not static over these timeframes (our on-ice base station was moving at a rate ~2 m d$^{-1}$). PPP kinematic processing for roving receivers is less accurate than kinematic relative differential carrier phase, achieving only sub-decimetre accuracy, and hence would have a downstream impact on photogrammetric product accuracy. Kinematic relative processing methods are modern standard best practice for rigorous in-situ GNSS data collection on the Greenland Ice Sheet, and with rigorous quality control have been used even up to 140 km from the ice margin/base station (Doyle *et al.* 2014). Further inland in an ice sheet environment, we would probably question the relevance of our technique anyway, as larger-scale seasonal patterns appear to dominate (*ibid.*). In an alternative slower-flowing environment, such as an alpine glacier, daily displacements are

17

probably low enough that a PPP kinematic method is a reasonable assumption. However, in such an environment, it would likely be the case that the base station is off the ice, in which case we would recommend falling back to the method we suggest for the calving front environment.

*14:4 the peak of which "is" centred*

Corrected.

*15:27 "moving one-ice GCP" should be "on-ice"*

Corrected.

*17:35 I think another point here is that dual frequency tends to provide more accurate positions on moving objects (i.e. UAV) especially in the vertical.*

Thanks for pointing out. This recommendation has been incorporated, alongside further changes to this paragraph recommended by reviewer #1, as follows:

L19P25-28 ...these GPS receivers are small and light enough to fit on small-sized UAV airframes, and hence allow for ... an improved flight baseline and accuracy

## References

Agisoft (2018). *Agisoft Photoscan User Manual: Professional Edition, Version 1.4*. https://www.agisoft.com/pdf/photoscan-pro_1_4_en.pdf (Accessed 2019-02-06)

Doyle, S. H., Hubbard, A., Fitzpatrick, A. A., van As, D., Mikkelsen, A. B., Pettersson, R., & Hubbard, B. (2014). Persistent flow acceleration within the interior of the Greenland ice sheet. *Geophysical Research Letters*, 41(3), 899-905.

Fazeli, H., Samadzadegan, F., & Dadrasjavan, F. (2016). Evaluating the potential of RTK-UAV for automatic point cloud generation in 3D rapid mapping. *The International Archives of Photogrammetry, Remote Sensing and Spatial Information Sciences*, *41*, 221.

King, M., Edwards, S., & Clarke, P. (2002). Precise point positioning: Breaking the monopoly of relative GPS processing. *Engineering Surveying Showcase*, 10(2002), 33-34.

King, M. (2004). Rigorous GPS data-processing strategies for glaciological applications. *Journal of Glaciology*, 50(171), 601-607.

Mian, O., Lutes, J., Lipa, G., Hutton, J. J., Gavelle, E., & Borghini, S. (2015). Direct georeferencing on small unmanned aerial platforms for improved reliability and accuracy of mapping without the need for ground control points. *The international archives of photogrammetry, remote sensing and spatial information sciences*, *40*(1), 397.

Roze, A., Zufferey, J. C., Beyeler, A., & McClellan, A. (2014). eBee RTK accuracy assessment. *senseFly White Paper*

Ryan, J. C., Hubbard, A. L., Box, J. E., Todd, J., Christoffersen, P., Carr, J. R., Holt, T. O., and Snooke, N. (2015). UAV photogrammetry and structure from motion to assess calving dynamics at Store Glacier, a large outlet draining the Greenland ice sheet, *The Cryosphere*, 9, 1-11.

Strick, R. J., Ashworth, P. J., Sambrook Smith, G. H., Nicholas, A. P., Best, J. L., Lane, S. N., ... & Dale, J. (2018). Quantification of bedform dynamics and bedload sediment flux in sandy braided rivers from airborne and satellite imagery. *Earth Surface Processes and Landforms*.

van der Sluijs, J., Kokelj, S., Fraser, R., Tunnicliffe, J., & Lacelle, D. (2018). Permafrost Terrain Dynamics and Infrastructure Impacts Revealed by UAV Photogrammetry and Thermal Imaging. *Remote Sensing*, 10(11), 1734.

Zollo, D., and Gohalwar, R. (2016) White paper: Piksi for UAV Aerial Surveying: RTK Direct Georeferencing with Swift Navigation's Piksi GPS Receiver. *Swift Navigation*

# High accuracy UAV photogrammetry of ice sheet dynamics with no ground control

Thomas R. Chudley[1], Poul Christoffersen[1], Samuel H. Doyle[2], Antonio Abellan[3], and Neal Snooke[4]

[1]Scott Polar Research Institute, University of Cambridge, Cambridge, UK
[2]Centre for Glaciology, Department of Geography and Earth Sciences, Aberystwyth University, Aberystwyth, UK
[3]Institute of Applied Geoscience, School of Earth and Environment, University of Leeds, Leeds, UK
[4]Department of Computer Science, Aberystwyth University, Aberystwyth, UK

**Correspondence:** Thomas R. Chudley (trc33@cam.ac.uk)

**Abstract.** Unmanned Aerial Vehicles (UAVs) and Structure from Motion with Multi-View Stereo (SfM-MVS) photogrammetry are increasingly common tools for geoscience applications, but final product accuracy can be significantly diminished in the absence of a dense and well-distributed network of ground control points (GCPs). This is problematic in inaccessible or hazardous field environments, including highly crevassed glaciers, where implementing suitable GCP networks would be logistically difficult if not impossible. To overcome this challenge, we present an alternative geolocation approach known as GNSS-supported aerial triangulation (GNSS-AT). Here, an on-board carrier-phase GNSS receiver is used to determine the location of photo acquisitions using kinematic differential carrier-phase positioning. The camera positions can be used as the geospatial input to the photogrammetry process. We describe the implementation of this method in a low-cost, custom-built UAV, and apply the method in a glaciological setting at Store Glacier in West Greenland. We validate the technique at the calving front, achieving topographic uncertainties of $\pm$ ~~0.07 m horizontally~~ 0.12 m horizontally ($\sim$1.1x the ground sampling distance) and $\pm$0.14 m vertically ($\sim$1.3x the ground sampling distance) when flying at an altitude of $\sim$450 m a.s.l. This compares favourably with previous GCP-derived uncertainties in glacial environments, and allowed us to apply the SfM-MVS photogrammetry at an inland study site where ice flows at 2 m ~~day~~d$^{-1}$ and where stable ground control is not available. Here, we were able to produce, without the use of GCPs, the first UAV-derived velocity fields of an ice sheet interior. Given the growing use of UAVs and SfM-MVS in glaciology and the geosciences, GNSS-AT will be of interest to those wishing to use UAV photogrammetry to obtain high-precision measurements of topographic change in contexts where GCP collection is logistically constrained.

## 1   Introduction

In recent years, Unmanned Aerial Vehicles (UAVs) have emerged as a versatile and practical tool for aerial surveying. A common application of this method that holds particular promise in the geosciences is the production of 3D topographic models from sequential 2D imagery using Structure from Motion with Multi-View Stereo (SfM-MVS) photogrammetry (Westoby et al., 2012; Fonstad et al., 2013; Eltner et al., 2016). With repeat surveys enabled through flight autonomy, SfM-MVS is creating new opportunities for the study of terrain evolution in 4D (James et al., 2017). The technique compliments, and

provides key advantages over, satellite-based earth observation methods, which have larger spatial coverage but lower spatial resolution, as well as an inherent trade off between spatial and temporal resolution in many applications. With a relatively low barrier of entry in terms of cost, UAV-derived photogrammetry is rapidly advancing and the versatility of the technique provides new avenues of research using additional image processing methods or on-board sensors, many of which have yet to

5   be explored. UAV-SfM has become an increasingly used tool within the cryospheric sciences (see Bhardwaj et al., 2016), in particular through the application of feature-tracking methods to multitemporal datasets in order to produce velocity datasets in glacial environments as diverse as the Himalaya (Immerzeel et al., 2014; Kraaijenbrink et al., 2016), Alps (Seier et al., 2017), Peruvian Andes (Wigmore and Mark, 2017), and the Greenland Ice Sheet (Ryan et al., 2015; Jouvet et al., 2017, 2018).

While UAV-derived photogrammetry offers key advantages over conventional surveying techniques in studies of 4D topo-
10   graphic change, the dependency on ground control points (GCPs) is often impractical and a hindering factor needed to scale and orient photogrammetric models to a real coordinate system (James and Robson, 2014; Carrivick et al., 2016). Previous work has shown that the quantity and distribution of GCPs can have a significant impact on the final accuracy of the photogrammetric products: for example, topographic error has been shown to increase if the number of GCPs is decreased and spacing between GCPs increases (Tahar, 2013; Johnson et al., 2014; James and Robson, 2014; Shahbazi et al., 2015; Tonkin
15   and Midgley, 2016). Accuracy assessments performed specifically for a glaciological environment report that for a ground sampling distance (GSD) of ∼6 cm, local accuracy decreases with the distance to the closest GCP at a rate of about 0.09 m per 100 m $^{-1}$ (Gindraux et al., 2017). Additionally, Gindraux et al. (2017) report an optimal GCP distribution density (i.e. beyond which no improvement in accuracy is observed for their GSD) of 7 GCP km$^{-2}$ for horizontal accuracy and 17 GCP km$^{-2}$ for vertical accuracy. Producing a GCP network of this density in glacial terrain can be impractical, logistically-expensive to col-
20   lect, and often unfeasible – as well as limiting one of the inherent advantages of UAVs in being able to remotely and accurately observe terrain which is difficult and hazardous to access on the ground. The difficulties of producing these networks can be observed in applied glaciological studies, where GCPs are often located only along the valley sides near a glacier's lateral margin (e.g. Immerzeel et al., 2014; Ryan et al., 2015). On-ice GCPs, if used, require repeat surveying as GCPs continuously advect with the glacier's flow. On fast-flowing glaciers (surface velocities of metres per day), these changes are so rapid that
25   GCP collection would need to be nearly contemporaneous with image acquisition to be effective for accurate geolocation – a requirement which is unfeasible for these glaciers due to crevasses forming on their surface. As a result of the difficulties in building GCP networks in glacial environments, alternative methods are often applied to externally constrain photogrammetric products. Such methods include using tie points to tie datasets together geodetically (Kraaijenbrink et al., 2016); linearly interpolating the on-ice GCP location from the beginning and end of a UAV campaign (Jouvet et al., 2017); or providing some
30   additional external constraint using an on-board navigational GPS geolocation (Ryan et al., 2015; Jouvet et al., 2017). The practical limitations of GCP collection is one of the most limiting factors in UAV-derived photogrammetry in the geosciences, especially in glaciological studies, where errors to date have been systematically larger than what is theoretically possible with this technique. Furthermore, these limitations have meant that no one has, to date, succeeded in using UAV-based methods to derive 4D surface evolution and velocity fields away from an ice sheet margin, where topographic ground-control is especially
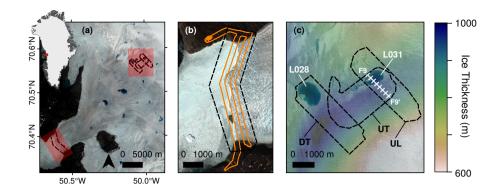35   scarce and often lacking altogether.

**Figure 1.** Location of study sites. (a) Store Glacier with calving front and inland study sites highlighted. Inset: location of Store Glacier in Greenland. (b) Calving front flight zone with example flight path shown. (c) Inland flight zones with labelled names: downstream transverse (DT), upstream longitudinal (UL), and upstream transverse (UT). Transect F9 marks location of fig. 9. Ice thickness from BedMachine v3 (Morlighem et al., 2017) is overlaid, and supraglacial lakes at the inland study site (L028 and L031) are also labelled.

~~Here, we show that the GCP dependency of SfM-MVS can be largely eliminated when~~ Recent developments in lightweight, low-cost GNSS technology have allowed for the proliferation of a new technique whereby differential carrier-phase GNSS positioning is used to ~~geolocate imagery acquired over a large Greenlandic outlet glacier with a fixed-wing UAV. Using this method~~ accurately geolocate imagery and subsequent photogrammetric products. This technique, known as GNSS-supported

5 ~~Aerial Triangulation (GNSS-AT; Hugenholtz et al., 2016; Benassi et al., 2017), we show that,~~ aerial triangulation (GNSS-AT; Benassi et al., has been shown to result in sub-GSD horizontal accuracy without the use of GCPs (Mian et al., 2015; Fazeli et al., 2016; Hugenholtz et al., Published applications of this technique in the geosciences are so far limited (van der Sluijs et al., 2018; Strick et al., 2018), and no studies yet examine the appropriateness of this technique for the study of glacial dynamics.

The aim of this paper is to: (i) apply GNSS-AT using a low-cost, custom-built airframe suitable for the study of extreme

10 environments; (ii) develop and describe modifications to the GNSS-AT process to allow surveys to be undertaken at inland ice sheet location far from suitable GPS reference stations; and (iii) validate the method for the study of glacier dynamics. Here, we demonstrate the suitability of GNSS-AT assisted UAV photogrammetry for ~~a GSD of ~11 cm, we can produce digital elevation models (DEMs) with an accuracy of ±0.07 m in the horizontal and ±0.14 m in the vertical, at low cost and without the dependency on GCPs. We demonstrate the capability of this technique for~~ assessing glacier dynamics using examples from

15 two specific settings where ~~GCP-based geolocation is~~ on-ice GCPs are not feasible. The first is the glacier's calving terminus, where deep fractures ~~prohibits~~ prohibit access, and bedrock exposure allows method uncertainty to be quantified; the second is the interior ice sheet where there is no exposed bedrock and therefore distributed ground control is prohibitively difficult.

## 2 Methods

### 2.1 Study site

Store Glacier (*Qarassap Sermia*, 70.4 ° N 50.6 ° W) is a marine-terminating outlet glacier in West Greenland. The third-fastest outlet glacier in Greenland, it has a 5.2 km wide calving front draining a ∼34,000 km² catchment (Rignot et al., 2008). The terminus of Store Glacier has been located in approximately the same position since at ~~last~~ least 1948 (Weidick et al., 1995), likely due to the presence of a prominent basal pinning point and the position of the terminus at a lateral valley constriction (Todd et al., 2018). The calving front of Store Glacier also marks the study site of ~~the seminal~~ a previous. application of UAVs to the study of glacial dynamics in Greenland by Ryan et al. (2015). Store's ice catchment extends 280 km from the calving front (Todd et al., 2018), and is underlain by an active subglacial hydrological system extending at least 30 km inland.

We surveyed two locations on Store Glacier: (i) at the calving front of Store, and (ii) at an on-ice site 30 km inland (Fig. 1). Our flights at the calving front were designed to test the GNSS-AT method, with exposed bedrock at the sides of the calving front providing good ground control for validation and error quantification. The location of our ~~four~~ primary inland flight zones were motivated by a subglacial bedrock trough visible in Bedmachine v3 data (Morlighem et al., 2017), which our flights profile longitudinally and transversely (Fig. 1c).

### 2.2 UAV platform and flight planning

We used a Skywalker X8 UAV (Figs. 2a, S1), an off-the-shelf fixed-wing air frame with a 2.12 m wingspan (Ryan et al., 2015; Jouvet et al., 2017). In a setup similar to the one used by Jouvet et al. (2017), we use open hardware "PixHawk" autopilot (https://pixhawk.org/) and APM Arduplane firmware (http://ardupilot.org/plane/) for flight control along a pre-programmed flight path. The UAV is capable of ~~a~~ ∼1 hour of flight time at a ∼60 km h⁻¹ cruising speed, although given our use case in an extreme environment, we flew conservatively for no more than 40 minutes. The ~~1 kg payload~~ total scientific payload weighs 500 g. This is includes a nadir mounted Sony α6000 24 MP camera with fixed 16 mm lens. To allow for direct georeferencing of each photo location, we included an on-board ~~Emlid Reach: a~~ lightweight L1 carrier-phase GNSS receiver ~~recording at a 5 Hz frequency~~ (an Emlid Reach, using a small Tallysman TW4721 antenna with a 100mm ground plane). The GNSS receiver was powered by the PixHawk autopilot, and recorded camera trigger events in the output RINEX data via a hot shoe trigger cable linked to the camera. The ~~complete setup was built for less than~~ cost of a complete flight unit (including frame, hardware, and scientific payload) was approximately ∼£1500 per unit. Further necessary ground equipment, which could be shared between units, came to ∼£300: this includes the radio transmitter and lithium polymer battery charger, but not the ground-based GPS (sections 2.3, 4.3).

The UAV flew autonomously along pre-defined flight routes designed on-site using Ardupilot's Mission Planner software. The 5m ArcticDEM mosaic (Porter et al., 2018) was used to assist with the flight path design, ensuring a constant relative altitude over the glacier and ~~allowing flight plans to avoid collision with cliffs when flying in steep terrain near the glacier's calving front~~ avoiding collision with high relief topography at the glacier margins. For each flight, the UAV flew a route autonomously at a relative altitude of ∼450 m above ground level, resulting in a ground-level footprint of ∼660 x 440 m and a

GSD of ~11 cm. ~~Out~~ Our camera was set to autofocus, and a fixed f-stop and ISO (between f/4–f/8 and ISO 100-400 respectively depending on lighting conditions) chosen to target a auto shutter speed of 1/1000 s. Photos were recorded in RAW format to ensure lossless storage of images, and converted into Photoscan-compatible 16-bit tiffs before processing. Flight lines were spaced ~250 m apart and the camera was set to trigger every ~80 m, typically acquiring ~300 images in an average flight.

5 These parameters ensured adequate overlap in the photographs for photogrammetry purposes, targeting 80% in the flight direction and 60% in the cross-flight direction. Flight paths in the ice sheet interior, where flight endurance allowed, also included a lower-altitude ~200 m along-track flightline with sharp banking turns designed to obtain imagery from multiple elevations and oblique angles. The aim of these lower-level flights was to reduce the potential vertical 'doming' effect on reconstructed surface topography that can occur when using self-calibrating bundle adjustment with image sets consisting of solely near-parallel

10 viewing directions ~~(James and Robson, 2014)~~(James and Robson, 2014; James et al., 2017; Nesbit and Hugenholtz, 2019).

## 2.3 GNSS-supported aerial triangulation

The block orientation process of SfM-MVS photogrammetry can be performed in two main ways (Benassi et al., 2017). The first is Indirect Sensor Orientation (InSO), where ground-based GCPs provide external constraints. The second is Direct Sensor Orientation (DSO, sometimes referred to as 'direct georeferencing'), where external orientation parameters are provided by

15 on-board systems including GNSS and an inertial measurement unit (IMU). Full DSO combines camera orientation data (e.g. from the IMU) with accurate camera location data from a GNSS receiver (see Cucci et al., 2017). Although DSO is not a new method for aerial photogrammetry (e.g. Blankenberg, 1992), InSO based methods have prevailed in UAV-based surveying, as the inexpensive navigational GNSS and IMU equipped in standard commercial UAVs are not accurate enough to provide more than metre-scale accuracy (James et al., 2017). Recently, commercial off-the shelf UAV units with DSO capability have become

20 available, although these remain expensive, often in excess of £20,000 for fixed-wing units at the time of writing. Here, we take advantage of the recent availability of low-cost, light-weight carrier-phase GNSS recievers to implement direct orientation for the first time in a glaciological study. The implementation described in this study is a subset of DSO referred to as GNSS-supported Aerial Triangulation (GNSS-AT), which requires GNSS data but not IMU data (Benassi et al., 2017). GNSS-AT is therefore well-suited to UAV applications where IMU data is not available or not accurate enough (e.g. where IMU data

25 is limited to that from lower-quality navigational units). GNSS-AT does, however, require position data that is more accurate than that provided by the GNSS receivers typically used for UAV navigation which use the Standard Positioning Service (SPS). Higher positioning accuracy than is offered by the SPS can be achieved by using differential carrier phase positioning, which makes use of the ability of GNSS receivers to measure the carrier phase to one hundredth of a cycle, equivalent to ~~2-3 mm~~ about 2 mm in distance (Leick, 2004).

30 To obtain accurate camera positions we ~~mounted a single-frequency (L1) Emlid Reach GNSS receiverinside the UAV. The receiver was configured to log continuously at~~ kinematically post-processed 5 ~~Hz and the data~~ Hz data logged by the on-board L1 carrier-phase GNSS receiver. Data were post-processed using the differential carrier phase kinematic program within Emlid's b27 fork of RTKLIB v. 2.4.3 software relative to a base station located at the launch site. Single-frequency receivers such as the Emlid Reach can be used for differential carrier-phase positioning for baselines on the order of kilometres
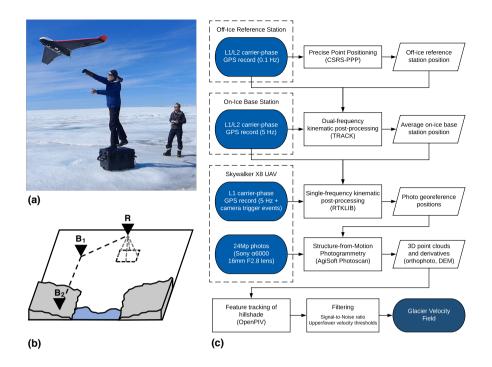
**Figure 2.** The method used in this study: (a) Launching the Skywalker X8 on the ice sheet; (b) cartoon ~~showing process~~ visualising the relationship of kinematic GPS corrections between the UAV rover (R), on-ice launch site base station ($B_1$), and the off-ice reference station ($B_2$); and (c) flowchart showing the workflow used in this study to derive photogrammetry products and velocity fields at the inland study site.

– distances over which the differential ionospheric delay is negligible. To apply differential corrections over the longer baselines as is often necessary in glacial environments, dual-frequency (L1/L2) receivers must be used to cancel out the frequency-dependent ionospheric delay. As dual-frequency GNSS receivers suitable for integrating in to the UAV were not available at the time of the survey (see section 4.3) we use single-frequency carrier phase positioning to determine the camera position ('R' in Fig. 2c) relative to a nearby base station ('$B_1$'), and dual-frequency carrier-phase positioning to determine the absolute position of the base station ('$B_1$') relative to a bedrock-mounted reference station ('$B_2$'). This method has the limitation that the UAV must stay within 10 km of the launch site base station, which may be located on or off the ice, but allows the launch site base station, and therefore the UAV flight, to be located long distances away from the bedrock-mounted reference station. In this study, ~~the~~ our base station (B1) was a Trimble R9s GNSS receiver (with Zephyr 3 antenna) located at the launch site, and the bedrock-mounted reference station ~~consisted of~~ was a continuously-operating Trimble NetR9 GNSS receiver (with Zephyr 3 Geodetic antenna) recording at 0.1 Hz located at Qarassap Nunata (70.4 ° N, 50.7 ° W), a mountain ridge near Store Glacier's calving front. For practical reasons and redundancy, we used this three-receiver set-up for all flights including those at the calving front, however, only one of the dual-frequency receivers was strictly required for flights at the calving front, where a bedrock-mounted base station was ~~achievable~~located nearby.

Whilst the Emlid Reach GNSS receiver is capable of real-time kinematic (RTK) ~~correction in combination with a radio link to a GNSS base station, our preferred option is~~ we used instead post-processed kinematic (PPK) positioning ~~. We chose PPK over RTK because the former~~ for three primary reasons. First, PPK does not rely on maintaining a reliable real-time radio link with a GNSS base station, which ~~limits the UAVs range from the base station and increases the UAVs payload and power consumption. Furthermore~~would introduce additional technical constraints. Second, PPK solutions are also often more accurate than RTK solutions as precise ephemeris data for the GNSS satellites is available during post processing. Third, absolute positioning using RTK requires a stationary reference station with a known position, which is not possible ~~away from the ice margin, as on-ice base stations advect with ice flow~~in real time on an advecting ice surface.

The overall workflow for photogrammetric reconstruction and for the generation of the glacier velocity field is illustrated in Figure 2c. First, the position of the Qarassap Nunata reference station was estimated using the average of 17 days of data collected at 0.1 Hz and processed with Precise Point Positioning (PPP) using the Natural Resources Canada Precise Point Positioning service (webapp.geod.nrcan.gc.ca/geod/tools-outils/ppp.php). Second, the position of the launch site base station was determined and for this two different methods were used depending on whether the base station was located on or off the ice. Where the base station was located on bedrock its position was determined using static differential carrier-phase positioning within RTKLIB 2.4.3 software. For flights at the ice sheet interior, the launch site base station was moving at approximately 1.5 m d$^{-1}$. We therefore processed this data kinematically (King, 2004) using the differential carrier phase positioning software Track v1.30 (Chen, 1998, http://geoweb.mit.edu/gg/). All GNSS processing used final precise ephemeris products from the International GNSS Service (Dow et al., 2009). We took the average position of the base station over the flight time as the absolute reference location. During the ∼20 minute flight period the base station could have moved by up to ∼2 cm, introducing a systematic error into the final calculated photo location. Given the small magnitude of this error relative to larger errors later in the workflow, we assume the interior base station data during the flight can be treated as stationary for post-processing purposes. Finally, we post-process the UAV-based data kinematically against the launch site base station data using Emlid's RTKLIB 2.4.3 b27 fork. The Emlid RTKLIB fork provides final photo geolocation using the GPS time of the camera trigger marker in the RINEX data by linearly interpolating between the two closest points of the 5 Hz record. ~~All GNSS processing used final precise ephemeris products from the International GNSS Service (Dow et al., 2009)~~RTKLIB camera location outputs are estimated to have standard deviations ∼0.6 mm horizontally and ∼1.1 mm vertically for fixed solution data.

## 2.4   SfM-MVS photogrammetry and feature tracking

SfM-MVS photogrammetry was performed with AgiSoft Photoscan (version 1.3.3; http://www.agisoft.com), using the determined camera positions in the input process. As geolocation was accurate to within millimetres, it was also necessary to include the directional offset between the receiver antenna and camera position (-7.9 cm in the Y direction and +13.2 cm in the Z direction relative to the lens of the camera) to properly locate camera centre points. Camera calibration was performed automatically in the bundle adjustment process, which is the preferred option when other variables of the bundle adjustment are

7

well constrained. From the final dense point clouds, we produce orthophotos at 0.15 m resolution and geoid-corrected DEMs at 0.2 m resolution based on recommended output resolutions from Photoscan.

We produced horizontal velocity fields by feature tracking 0.2 m resolution multidirectional hillshade models produced from the DEMs using GDAL 2.2. Using DEM-derived products has the disadvantage of having a slightly lower resolution than an orthophoto, but the advantage of being consistently comparable when tracking datasets collected in variable lighting conditions. In particular, orthophotos acquired at different times of the day can complicate feature tracking due to the variation in shadow directions (cf. Jouvet et al., 2017). To feature track images, we used OpenPIV (Taylor et al., 2010), an open-source particle image velocimetry software implemented in MATLAB. Following a sensitivity analysis, we chose an optimal interrogation window size of 320x320 pixels and a spacing of 32 pixels, resulting in a final resolution of 6.4 m. After the production of the velocity field, we filtered erroneous values using manually chosen upper and lower thresholds for both velocity and signal-to-noise ratio (SNR) - generally between 0.8-1.1 at the lower bound and 2.8-3.5 at the upper bound.

## 2.5 Uncertainty assessment

Relative uncertainties were calculated by assessing inter-DEM variation in the elevation of the exposed bedrock on Qarassap Nunata near the calving front, assuming no expected change in topography. Vertical uncertainty ($\sigma_z$) was calculated by assessing the mean per-pixel standard deviation from the mean elevation of the repeat DEMs. Horizontal uncertainty ($\sigma_{xy}$) was ~~derived from~~ estimated using feature-tracked displacement fields. First, we calculate the root mean square error in displacement fields ($s_{RMSE}$) produced in the feature tracking process (Ryan et al., 2015). We ~~then calculate the horizontal uncertainty in an individual model from displacement error identified by modifying standard satellite-based velocity uncertainty equations (McNabb et al., 2012; Quincey et al., 2015)~~ assume that this value results from the combined error from the root mean square error of the two tracked images. Hence, we ~~obtain:~~

$$C_{pix} = \frac{s_{RMSE}}{\Delta x} - C_{match}$$

~~,~~

where ~~$C_{pix}$ is~~ estimate the horizontal uncertainty ~~in pixels, $C_{match}$ is the uncertainty in the feature tracking algorithm, for which we use a typical value of 0.5 pixels, and $\Delta x$ is the raster resolution in metres. Hence, ($\sigma_{xy}$ can be calculated by multiplying $C_{pix}$ by the pixel resolution (0.2 m).~~ ) as follows:

$$\sigma_{xy} = \sqrt{\frac{s_{RMSE}^2}{2}} \tag{1}$$

Note that this estimate ignores potential error contributions from feature tracking in $s_{RMSE}$, and hence likely only provides an upper bound on the horizontal uncertainty.

From $s_{RMSE}$, we can also calculate the uncertainty of any horizontal velocity field ($\sigma_v$) as follows:

$$\sigma_v = \frac{s_{RMSE}}{\Delta t} \tag{2}$$

where $\Delta t$ is the time interval of the velocity field.

5      As our external orientation parameters (camera positions) are distributed densely, consistently, and evenly throughout the point cloud (cf. a GCP-based network), we assume that error is spatially non-variable, and hence that uncertainties measured at the bedrock margins are representative of error across the SfM-MVS product.

## 3    Results

### 3.1    Calving front

10   #### 3.1.1    DEMs and velocity fields

The calving front of Store Glacier was surveyed ten times between 10th-14th July 2017 (Table S1). Typical UAV-derived glaciological products for the calving front are shown in Figure 3, including orthophoto, DEM, and velocity field.

Our method reproduces both small- and large-scale aspects of the calving front in fine detail. At glacier-wide scales, the side of the calving front is known to have a prominent surface depression, an expression of a retreated grounding line and section of

15   the front at floatation (e.g. Ryan et al., 2015; Todd et al., 2018). This is captured well by the GNSS-AT photogrammetry (Figure 3a)b; 4a). At local scales this method is accurate enough to capture the opening of crevasses over periods of days (Figure 4b; 5d–e), although reconstruction of crevasse depth continues to be problematic due to low illumination and inefficient sensor orientation within crevasses (Ryan et al., 2015).

The GNSS-AT method can also be successfully used to derive velocity fields of the calving front at high resolution and

20   accuracy (Fig. 3b; 4a). The velocity field, derived from displacements detected over an a six-hour period between 16:15 and 22:15 on the 12th July 2017 ($\sigma_v = 0.69$ m d$^{-1}$), shows that velocities are generally uniform (15 m d$^{-1}$) across much of the central calving front, with localised peaks of 20 m d$^{-1}$ .(Fig. 3c; 4a; 5h). Our method is sensitive to small changes occurring dynamic changes at the calving front: in particular, the areas of highest velocity at the very lip of the calving front – such as regions ~1.8–2 km and ~5.2–5.4 km along profile A (Fig. 4) – all mark areas of ice that undergo calving events in the next 24–48

25   hours. One particular calving event, occurring between 22:15 on the 12th July and 10:15 on the 13th July on the southern side of Store Glacier, is detailed in Figure Figures 4b and 5. The calving zone, measuring ~65,150 000 m$^2$, occurs in a region of high shear strain in a region bordering the floating section of Store. More the than 48 hours before calving, deformation in the calving zone is anomalous relative to the surrounding area: up to 20 m d$^{-1}$, whilst the region immediately behind the zone is <10 m d$^{-1}$ (Fig. 5dg). Over the following two days, a plume becomes visible in front of the calving zone, opening up a region

30   of open water in the ice melange (Fig. 5a–c). a–b). The crevasse becomes deeper and wider during this time (Fig. 4b): across
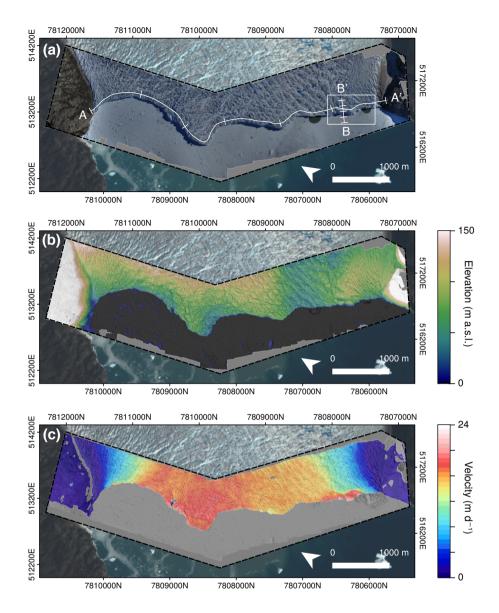
**Figure 3.** Example data output from calving front. (a) 0.15 m orthophoto, collected 10:15 12th July 2017. (b) 0.2 m DEM from same flight. (c) 6-hour ~~seperation~~ separation velocity field ($\sigma_v = \pm0.69$ m) from 16:15–22:15 on the 12th July. Transects in (a) refer to Figure 4. Box refers to location of Figure 5

transect B-B' (Fig. 3a), the crevasse increases from ~57.5 m wide and ~19.2 m deep at the first observation (2017-07-10 12:30) to ~73.5 m wide and 49.6 m deep at the final observation before calving (2017-07-12 22:20). The crevasse is not obviously water filled in this period (Fig. 5b), but is filled with ice debris that has dry calved off the interior face of the crevasses (Fig. 4b; 5b), so the depths are reported above are underestimated, and water may exist beneath the debris. In the hours prior to calving,
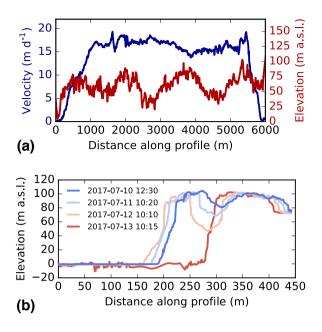
**Figure 4.** (a) Transect of A-A' in Figure 3(a), displaying velocity (blue) and elevation (red). (b) Transect of B-B' in Figure 3(a), displaying elevation profiles of the calving front through the study period. A ~~large-scale~~ calving event occurs between the ~~13~~12th and ~~14~~13th of July.
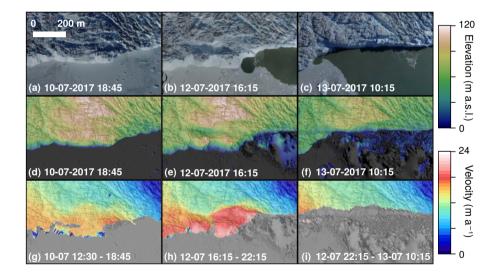


**Figure 5.** Orthophotos (a–c), DEMs (d–f) and velocity fields (~~d–f~~e–i) showing the lead-up and aftermath of a calving event that occurred on the south side of Store Glacier between 22:15 on the 12th July and 10:15 on the 13th July. Location is marked by outline in Figure 3a. NB. the poor reconstruction of open water visible in DEMs and hillshades of figures e, f, h, and i.
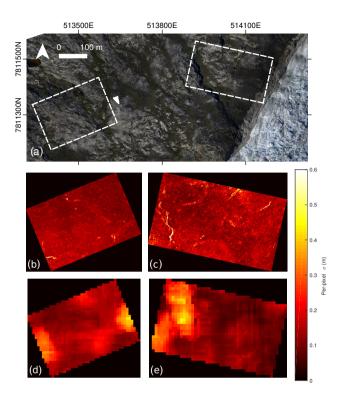
**11**

**Figure 6.** Error assessment at the calving front: (a) location of two validation sites at the calving front shown on UAV-derived orthophoto; (b-c) standard deviation in Z axis derived from DEMs (d-e) standard deviation in XY axes derived from horizontal displacement fields.

the calving zone reaches deformation rates ~~in excess~~ up to 24 m d$^{-1}$ ~~, before returning to~~ (Fig. 5h). The calving event itself resulted in the loss of an ice section ~400 m in length extending ~100 from the front of the glacier. Assuming the calving front is at floatation in this region of the glacier front (Todd et al., 2018), we estimate from elevation models that the total ice lost to be 9.5 x 10$^7$ m$^3$ (~0.1 km$^3$). After calving, displacement rates at the glacier fronts return to levels consistent with the surrounding area ~~after calving occurs~~ (Fig. 5~~d – e~~i).

### 3.1.2 Uncertainty analysis

To estimate the error of the technique, we sampled a total of 0.1 km$^2$ of bedrock across two zones close to the glacier margin where reconstruction quality matched that of the glacier surface across all DEMs (Fig. 6a). We selected eight DEMs and eight displacement fields of these sample areas, produced by feature tracking consecutive hillshaded DEMs.

The uncertainties derived from assessment of these DEMs is $\sigma_z = \pm 0.14$ m and $\sigma_{xy} = \pm$~~0.07 m, with an s$_{RMSE}$ of $\pm$0.17 m.~~ 0.12 m. This amounts to ~1.1 times the GSD (~11 cm) in the horizontal and ~1.3 GSD in the vertical. The per-pixel standard deviation in the vertical axis (Fig. 6b–c) shows that vertical deviation is relatively consistent across the image. The areas of highest deviation (visible as bright yellow-white bands in Figure 6c) are pixels that are located at steep topographic cliffs,

where slopes are close to vertical and thus any horizontal error will compound the reported deviation in the vertical axis. The per-pixel standard deviations in the horizontal (Fig 6d–e) ~~reveals~~ reveal clustered 'hotspot' regions of high variation. However, close inspection of individual displacement fields shows that these hotspots are an artefact of individual anomalies in the displacement fields, and that areas of high deviation are not spatially consistent between displacement fields. Hence, although horizontal uncertainty is spatially variable, the variability is not dependent on factors such as surface texture or roughness, which would invalidate the assumption that a single uncertainty value can be assigned uniformly to an entire DEM.

With a displacement uncertainty $s_{RMSE} = 0.17$ m ($\sim$1.5 GSD) and the ability to capture ice flow accurately, even along the relatively slow moving (1-5 m d$^{-1}$) sides of the glacier calving front, these uncertainty tests validate our ability to use GNSS-AT derived UAV-photogrammetry to produce accurate DEMs and velocity fields of the ice sheet interior, where there are no exposures of bedrock and ice flow is considerably slower. Because feature tracking was able to successfully track displacements of <~~1 m~~5 pixels, the same hardware and methodological approach should be sufficient to identify daily displacements at inland sites up to $\sim$60 km from the calving front of Store Glacier (i.e. to the 1 m d$^{-1}$ velocity contour).

## 3.2   Ice sheet interior

The interior study area is located 30 km inland from the calving front, where ice flows at a speed of 2 m ~~/day~~ d$^{-1}$. The location of the flight paths was motivated by the presence of a large subglacial trough identified in BedMachine v3 data, and the presence of two supraglacial lakes 28 and 31 km inland (Lake 028 and Lake 031 – see Fig. 1c). Typical UAV-derived glaciological products for the ice sheet interior (flight zone 'DT' – see Figure 1c for location) are shown in Figure 7, including orthophoto, DEM, and velocity field.

Although flight zone DT was designed to capture Lake 028, it is apparent from orthoimagery that the lake had drained prior to the beginning of the study (Fig. 7). Sentinel-2 imagery shows the drainage to occur between the 19th June and the 7th July, although Lake 031 remained filled during the study period. Lake 031 overflows into a supraglacial stream which terminates in a large (>10 m diameter) moulin formed from the hydrofracture of Lake 028. This distinct hydrological network is visible in the former lake bed (Fig. 7a), which is clearly seen as a depression in the surface DEM produced by SfM-MVS (Fig. 7b). Figures 7a–b capture two historical features of lake drainage. The first is the fracture and moulin from the 2017 lake drainage, as already described. The second is the remnant lake ice from the 2016 lake, which did not drain and is still visible as a lighter patch of ice in the ~~west~~ western corner of Figure 7a.

Figure 7c shows a velocity field derived by feature tracking displacements on two DEM hillshades produced from orthophotos with four days seperation, from 22nd – 26th July 2017 ($\sigma_v = 0.05$ m d$^{-1}$). To our knowledge, this represents the first published UAV-derived velocity field of an ice sheet interior, constructed without the use of GCPs. Feature-tracking has successfully reconstructed the full range of velocities across the interior region in which ice flow gradually increases from $\sim$1.4 m d$^{-1}$ in the west to $\sim$2.4 m d$^{-1}$ in the east (Fig. 8a). We interpret this difference to occur due to differences in bedrock topography: to the southeast, ice is flowing over a bedrock rise, the peak of which is centred approximately 2 km southeast of the study region (Fig. 1). This change in dynamics is expressed in the ice surface as an increasing frequency of deep and open crevasses (Fig. 7a; 8b).
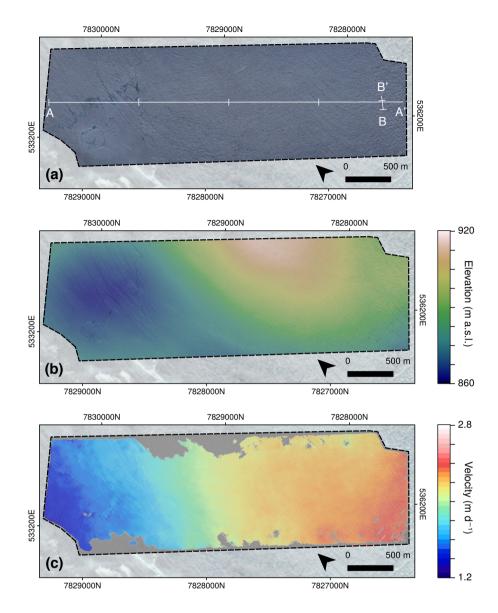
**Figure 7.** Example data output from the ice sheet interior. (a) 0.15 m orthophoto collected 15:15 22$^{nd}$ July 2017. (b) 0.2 m DEM from the same flight. (c) Velocity field ($\sigma_v = \pm 0.05$ m) from 15:15 22$^{nd}$ – ~~09~~19:30 26$^{th}$ July 2017

~~Although the lack of stable bedrock means that error cannot be assessed as in section 3.1.2, we can test for robustness~~ We can test the robustness of the inland surveys by comparing contemporaneous velocity fields from independent ~~surveys~~flights. Figure 9 shows a 1.4 km velocity profile of two velocity fields, constructed for the same time period (22$^{nd}$ – 26$^{th}$ June) but from two different flight paths (paths UT and UL in Fig. 1c). Despite being derived from entirely different datasets, the velocity products

5     show remarkable agreement as they clearly fall within our estimated $\sigma_v$ uncertainty of $\pm 0.05$ m d$^{-1}$ (section 2.5). Hence,
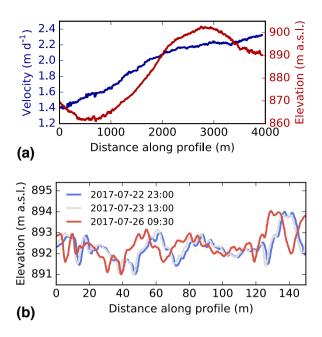
**14**

**(a)**



**(b)**

**Figure 8.** (a) Transect of A-A' in Figure 7(a), displaying velocity (blue) and elevation (red). (b) Transect of B-B' in Figure 7(a), displaying elevation profiles of a crevasse field through the study period.
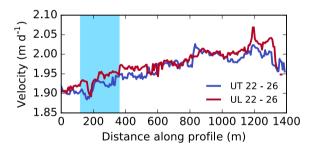


**Figure 9.** Comparison between two velocity fields obtained from different flight paths at comparable times between the 22$^{nd}$ and 26$^{th}$ July 2017. Blue shading marks where the transect crosses Lake 031. Transect is visualised as transect F9 in Figure 1c.

cross-comparison of different datasets appears to show that velocity products are robust between varying SfM-MVS input data. Additionally, the velocity products appear to be consistent even when tracking features through water, when tracking through Lake 031 (Figure 10). Thus, although refraction at the water surface influences SfM photogrammetry in the z-axis without corrective measures (e.g. Mulsow et al., 2018), these data suggest that the horizontal accuracy of bathymetry generated

5 by SfM-MVS photogrammetry is sufficient to ~~detect ice flow through~~ measure horizontal displacement through (non-turbid) water such as supraglacial lakes.

## 4 Discussion

### 4.1 Comparison with prior methods

In this study we have ~~shown~~ estimated that, in a glacial environment flying at ~~±~~~450 m above ground level, SfM-MVS photogrammetric products supported by GNSS-AT geolocation can be accurate to ±~~0.07 m in the horizontal~~ 0.12 m (~1.1 GSD) and ±0.14 m ~~in the vertical. Thus, feature tracking can be~~ (~1.3 GSD) in the horizontal and vertical respectively. With well-constrained geolocation, horizontal (vertical) accuracies can be as high as 0.5-1.0 GSD (1.5-2.0 GSD) (Benassi et al., 2017). Our estimated accuracies are very close to these theoretical values – in fact, our vertical accuracy is even higher. Our lower accuracy in the horizontal is likely due to the fact that $s_{RMSE}$ includes feature tracking error. Common estimates of the latter can be up to 0.5 pixels (e.g. Quincey et al., 2015), which if assumed in our use case would bring the $\sigma_{xy}$ estimate down as little as ~0.5 GSD. Our estimated accuracy values agree well with previously reported GNSS-AT derived estimates. For instance, Fazeli et al. (2016) report horizontal (vertical) accuracies of 0.6 (1.0) GSD using a low-cost customised multirotor UAV. Our accuracies also align with reported horizontal (vertical) accuracies of commercial fixed-wing drones, which offer similar performance to our low-cost alternative at a considerably higher price. Studies using the eBee RTK have reported horizontal (vertical) accuracies of 1.0 (1.2) GSD (Roze et al., 2014), and 0.6-1.2 (0.8-4.0) GSD (Benassi et al., 2017), and 0.8 (1.8) GSD (van der Sluijs et al., 2018), whilst the WingtraOne PPK has reported horizontal (vertical) accuracies of 1.3 (2.3) GSD (Ng and Buchheim, 2018). As a result of this level of accuracy, feature tracking can be used to reliably resolve decimetre-scale ~~displacements~~ displacement ($s_{RMSE}$ = 0.17 m, ~1.5 GSD) in the ice surface without the use of GCPs. For the investigation of glacier dynamics, where installing and surveying GCPs is logistically demanding, GNSS-AT therefore represents an especially significant technical advance. The method reported here can be directly compared to analogous UAV studies of Greenland glacier dynamics where both methods and uncertainty assessments have been rigorously reported.

The first example is that of Ryan et al. (2015) for Store Glacier, who were amongst the first to use UAVs in a study of Greenland Ice Sheet dynamics. Ryan et al. (2015) geolocate imagery in a two-stage procedure. First, external calibration in the SfM-MVS process was performed camera coordinates provided by an on-board autopilot navigational GPS reciever, which had an accuracy ±5 m. ~~This~~ Flying at ~500 m a.s.l. (GSD ~0.18 cm) provided a DEM with relative errors up to ±17.12 m horizontally (~95.5 GSD) and ±11.38 m vertically (~63.2 GSD), with notable warping in sea-level. A secondary stage of processing used a single GCP at the glacier margin, 3D co-registration of DEMs using visible common control points such as boulders and promontories, as well as a number of sea level control points given nominal values of zero m a.s.l.. These secondary step reduced measured RMSE across bedrock margins to ±1.41 m horizontally (~7.8 GSD) and ± 1.90 m vertically (~10.6 GSD). Hence, Ryan et al. (2015) show that it is possible to achieve scientifically valuable results even without strong ground control. However, an error >1 m ~~d$^{-1}$~~ is of limited use to assess displacement on slower-flowing glaciers, or over short time periods – indeed, the velocity fields of Ryan et al. (2015) have notable artefacts in slow-flowing (<5 m d$^{-1}$) sectors of the calving front. The GNSS-AT method shown here provides an order-of-magnitude improvement in accuracy, as well as eliminating an additional processing step. Despite ~~tracking displacement over~~ this study using a shorter time interval between flights (6 hours compared to 24 hours) ~~,~~ – and hence evaluating velocity from a smaller magnitude of displacement – the

**16**

velocity fields in this study are more accurate, permitting detection of changes in the slow-flowing sections of the ice margin. The method also successfully reconstructs a flat sea level (this can be seen in ~~detail~~ the first three transects displayed in Figure 4b – the final transect is disrupted by poor reconstruction of open water). The previous failure to reconstruct a flat sea surface of constant elevation in the first processing pass of Ryan et al. (2015) is likely a 'bowing' effect from radial lens distortion

5    error in the fixed or self-calibrated camera calibration (James and Robson, 2014), a feature that can be reduced significantly with ~~the introduction of accurate aerial~~ precise georeferencing (James et al., 2017).

Further work on UAV dynamics studies of calving fronts was developed by Jouvet et al. (2017, 2018) for Bowdoin Glacier in North Greenland. They report an improved horizontal ~~error~~ accuracy of 10-20 cm ($\sim$1.4-2.9 GSD), a value that improves on Ryan et al. (2015), and approximately double that in this study. They achieve this level of accuracy using ~~two~~ ten GCPs on

10   each side of the 3 km-wide calving front, as well two GCPs on the glacier surface recorded using repeat dGPS positioning, with absolute positions of on-ice GCPs during each flight linearly interpolated. They also fly at a lower altitude ($\sim$300 m a.s.l.; GSD $\sim$7 cm) than that of Ryan et al. (2015) and this study (400-500 m a.s.l.), which improves the quality of photogrammetric reconstruction whilst limiting the total area able to be assessed in a single flight (Bowdoin is $\sim$3 km across, whilst Store is $\sim$5 km). Hence, Jouvet et al. (2017, 2018) show that it is possible to work with moving ~~one ice~~ on-ice GCPs to provide viable

15   products. However, the logistical effort is still considerable, and as a result GCP density is sparse, with large distances (up to 2 km) between GCPs, which likely leads to significant errors at points far from GCP location (Tonkin and Midgley, 2016; Gindraux et al., 2017). Additionally, linearly interpolating moving GCPs on the calving front: (i) ~~assumes~~ requires that the calving front is a safe space to operate in logistically; and (ii) assumes that the glacier is moving at a constant velocity, which is a non-optimal assumption especially when studying glacier dynamics. The GNSS-AT approach applied here allows for the

20   ability to resolve decimetre-scale displacements without depending on a GCP network. This resolves large logistical challenges at marine-terminating calving fronts, where collecting GCPs on both sides of the calving front and on the ice itself would likely require a safe operating environment, considerable time investment, and/or helicopter access, all of which are downsides that UAVs are in some way meant to alleviate.

Whilst the method described here greatly reduces the logistical requirements of working with a network of GCPs, it does not

25   ultimately change the nature or limitations of the SfM-MVS process. For instance, the identification of key points or common features during the 3D reconstruction process will still struggle to reconstruct low texture environments such as fresh snow (Gindraux et al., 2017) or open water (visible in ~~the hillshade of Figure 3f cf. 5e~~ Figure 5e–f and the final transect of Figure 4b), as well as the true depth of crevasses (Ryan et al., 2015). Image collection should still be conducted according to best practice, including careful consideration of image overlap and flight geometry (James and Robson, 2014).

30   **4.2 Applications**

The case studies of a calving front and ice sheet interior provided in this study show two different applications of the GNSS-AT method: one in a calving front environment where UAVs have previously been used, and one in an ice sheet interior, where UAVs have not to date been used to assess ice dynamics. The first case study highlights that existing observations of, for instance, calving events (Ryan et al., 2015; Jouvet et al., 2017, 2018) can be successfully replicated using GNSS-
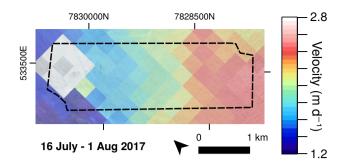
**17**

**Figure 10.** Landsat 8 OLI-derived velocity field of the study area between 16th July and 1st August 2017. Data is from GoLIVE project (Fahnestock et al., 2016, resolution = 300 m), overlaid onto Sentinel-2 optical imagery. Black outline marks the ~~extend~~ extent of the study zone in Fig. 7. Note that feature tracking has failed over the site of the former ~~lakebed~~lake bed.

AT methods (Fig. 5). However, the second case study, deriving surface velocity of an ice sheet interior, has not previously been possible using UAV-SfM methods. Instead, UAV-based ice sheet studies have largely focused on non-dynamic aspects of surface glaciology, such as albedo (e.g. Ryan et al., 2017; Burkhart et al., 2017).

Inland, opportunities for measurement of ice velocity are currently restricted to either: high-resolution in-situ GNSS mea-
5  surements (e.g Doyle et al., 2015), which can capture ice velocity at extremely high temporal resolution and accuracy but only for point measurements; or satellite remote sensing techniques (e.g. Tedstone et al., 2015), which can offer regional coverage at the expense of spatial and temporal resolution (and often an inherent trade-off between the two). The opportunity for broad spatial coverage of ice velocity at high temporal resolutions (e.g. daily) is extremely limited, and often restricted to opportunistic or targeted observations where repeat intervals occur at adequate frequencies (e.g. Palmer et al., 2011; Minchew et al.,
10  2017). UAV-based techniques allow for high-resolution velocity fields to be obtained by field researchers in targeted areas without dependency on high temporal resolution satellite observations, and with a much higher quality product than that available from global datasets and products. This quality improvement is apparent when we compare the inland velocity product in this study to a GoLIVE (Landsat-8 derived) product (Fig. 10; Fahnestock et al., 2016). While the satellite-derived data captures the overall variation of ice flow in the study region, the acceleration from west to east is considerably less detailed. The reduced
15  temporal resolution (16 days) results in a failure of the feature tracking algorithm to capture changes over the former lake bed, where changes in the supraglacial hydrological network ~~has negated cross-correlation 10~~disrupted feature tracking (Fig. 10). The ability to create field-based velocity fields provides new opportunities to study the spatial variation in short-term (daily-weekly) velocity variations on ice sheets, such as those provided by supraglacial lake drainages, or variation in moulin inputs in response to rainfall or melt events.

20  **4.3  Future directions**

Although our method shows an improvement in accuracy relative to prior glaciological studies, this is in part due to the sub-optimal GCP placement of prior studies that is a necessary by-product of working in glacial environments where access is

**18**

restricted in many places. When optimally arranged, Benassi et al. (2017) show that a dense network of ground control points still provides a better accuracy than GNSS-AT methods, particularly vertically (∼30% improvement in the horizontal and ∼60% in the vertical). However, it has been shown that the error of a GNSS-AT-derived product can be further constrained by the reintroduction of at least one GCP, with a final vertical accuracy only slightly worse than traditional GCP networks (Benassi

5    et al., 2017). Whilst constructing a comprehensive network of GCPs might be difficult on glacial terrain, the introduction of one GCP, either in the form of an existing continuous GPS station, or a single target measured on a per-flight basis or interpolated linearly as per Jouvet et al. (2017, 2018), is far more achievable than a large, dense network of GCPs. The method as described here also lacks the incorporation of directional data in the camera coordinate positions, and hence is referred to as GNSS-AT rather than full DSO (section 2.3). The navigational IMU on-board the autopilot was not precise nor accurate enough with

10   regards to time tagging to allow full DSO. The introduction of a more precise IMU – analogous to the improvement in precision between SPS and PPK geolocation in this study – would allow full DSO geolocation in the SfM-MVS process (Cucci et al., 2017) using a low-cost UAV system. However, we are not aware of any applied use of UAV-based DSO in the geosciences at the time of writing.

The UAV system and payload used in this study can be constructed for under £1500, which means our core hardware pushes

15   the boundary of UAV applications in polar and other extreme environments whilst conforming to the low-cost ethos of much geoscientific UAV work. However, the full method we have described here deviates from that ethos by virtue of the dependence on dual-frequency carrier-phase GNSS base station receivers for the differential processing of GPS data, which can often have high costs. Dual-frequency recievers are necessary for carrier phase GNSS correction over distances > 10 km, and hence as long as the UAV is equipped with a single-frequency receiver, there is a necessity for a local (< 10 km) base station to be running in

20   parallel during the flight period. Fortunately, there has been a recent availability of cost-efficient (< USD1000) dual-frequency receivers such as the Piksi Multi (https://www.swiftnav.com/), the Tersus BX305 and BX316R (https://www.tersus-gnss.com/), and the ComNav K501G and K708 (http://www.comnavtech.com/). These receivers present three potential innovations on the method presented here. Firstly, the integration of these ~~systems allows for the realisation of a truly low-cost, GCP-free UAV-MVS workflow for glaciological applications. Secondly, these receivers are~~ low-cost systems would reduce the initial

25   capital cost of projects that do not already have access to an expensive dual-frequency GPS receiver. Second, these GPS receivers are small and light enough to fit on small-sized UAV airframes, ~~allowing for on-board dual-frequency GNSS receivers, and hence an extension of the GPS baseline (and therefore potential flight range) compared to single-frequency systems. This improvement would remove the necessity for a launch site base station (B$_2$ in Fig. 2~~and hence allow for (i) an improved flight baseline and accuracy, and (ii) direct kinematic correction against an off-ice reference station (i.e. the removal of the need for

30   processing the intermediate base station 'B1' in ice sheet environments). Finally, these receivers could act as affordable on-ice base stations that could be distributed with a high enough density to act as ~~affordable continuous~~low-cost 'continuous' on-ice GCPs, allowing for reduced error (as above) and validation of the final point cloud output.

## 5 Conclusions

We have presented the application of an alternative SfM-MVS geolocation method known as GNSS-supported aerial triangulation, which uses an on-board carrier-phase GNSS receiver to geolocate SfM-MVS point clouds while significantly reducing the need for GCPs. Using the calving ice front of a large Greenlandic outlet glacier as a test case, we have shown that uncertainties in the reconstruction of the glaciers surface can be reduced to ±~~0.07 metres horizontally~~ 0.12 metres horizontally (∼1.1 GSD) and ±0.14 m vertically (∼1.3 GSD), when flying at ∼450 m above ground level. These values compare favourably with those obtained in previous studies, which used networks of GCPs for geolocation. The elimination of ground control allows us to assess ice displacement at an inland site and to produce, to our knowledge, the first example of velocity fields derived from UAV methods at an ice sheet interior site.

The nature of studies of glacial environments inherently limits the ability of users to collect dense networks of GCPs. GNSS-AT will be of interest to those wishing to use UAV photogrammetry to obtain high-precision measurements in all glacial contexts, but will be of particular value for operation in the interior of larger ice masses, such as ice sheets, where operation away from exposed bedrock makes the collection of stable GCPs a nearly impossible task. This method has further applications, both within studies of the cryosphere – for example, in studies of sea ice – but more broadly in all geoscience applications where UAV operation occurs in hazardous environments.

*Data availability.* All derivative data used in this study (orthophotos, DEMs, velocity fields) are available upon request. Please contact Tom Chudley for this purpose (trc33@cam.ac.uk). Full source data will be made available in an online repository at the conclusion of the ERC RESPONDER project.

*Author contributions.* TRC and PC designed the study. TRC designed the UAV payload, built the UAVs, processed the GPS rover data, and processed and analysed the photogrammetry data. SHD advised on GPS techniques, collected and processed the GPS reference and base station data, and assisted with GPS rover processing. AA assisted with flight path design and photogrammetric processing. NS originally designed the UAV and helped to build the units used in this study. TRC wrote the paper with input from all authors.

*Competing interests.* The authors declare that they have no conflict of interest.

# References

Benassi, F., Dall'Asta, E., Diotri, F., Forlani, G., Morra di Cella, U., Roncella, R., and Santise, M.: Testing Accuracy and Repeatability of UAV Blocks Oriented with GNSS-Supported Aerial Triangulation, Remote Sensing, 9, 172, https://doi.org/10.3390/rs9020172, 2017.

Bhardwaj, A., Sam, L., Akanksha, Martín-Torres, F. J., and Kumar, R.: UAVs as remote sensing platform in glaciology: Present applications and future prospects, Remote Sensing of Environment, 175, 196–204, https://doi.org/10.1016/j.rse.2015.12.029, 2016.

Blankenberg, L. E.: GPS-supported aerial triangulation - state of the art, The Photogrammetric Journal of Finland, 13, 4–16, 1992.

Burkhart, J. F., Kylling, A., Schaaf, C. B., Wang, Z., Bogren, W., Storvold, R., Solbø, S., Pedersen, C. A., and Gerland, S.: Unmanned aerial system nadir reflectance and MODIS nadir BRDF-adjusted surface reflectances intercompared over Greenland, The Cryosphere, 11, 1575–1589, 2017.

Carrivick, J. L., Smith, M. W., and Quincey, D. J.: Structure from Motion in the Geosciences, John Wiley & Sons, 2016.

Chen, G.: GPS kinematic positioning for the airborne laser altimetry at Long Valley, California, Ph.D. thesis, Massachusetts Institute of Technology, 1998.

Cucci, D. A., Rehak, M., and Skaloud, J.: Bundle adjustment with raw inertial observations in UAV applications, ISPRS Journal of Photogrammetry and Remote Sensing, 130, 1–12, 2017.

Dow, J. M., Neilan, R. E., and Rizos, C.: The international GNSS service in a changing landscape of global navigation satellite systems, Journal of geodesy, 83, 191–198, 2009.

Doyle, S. H., Hubbard, A., van de Wal, R. S. W., Box, J. E., van As, D., Scharrer, K., Meierbachtol, T. W., Smeets, P. C. J. P., Harper, J. T., Johansson, E., Mottram, R. H., Mikkelsen, A. B., Wilhelms, F., Patton, H., Christoffersen, P., and Hubbard, B.: Amplified melt and flow of the Greenland ice sheet driven by late-summer cyclonic rainfall, Nature Geoscience, 8, 647–653, https://doi.org/10.1038/ngeo2482, 2015.

Eltner, A., Kaiser, A., Castillo, C., Rock, G., Neugirg, F., and Abellán, A.: Image-based surface reconstruction in geomorphometry–merits, limits and developments, Earth Surface Dynamics, 4, 359–389, 2016.

Fahnestock, M., Scambos, T., Moon, T., Gardner, A., Haran, T., and Klinger, M.: Rapid large-area mapping of ice flow using Landsat 8, Remote Sensing of Environment, 185, 84–94, 2016.

Fazeli, H., Samadzadegan, F., and Dadrasjavan, F.: Evaluating the potential of RTK-UAV for automatic point cloud generation in 3D rapid mapping, The International Archives of Photogrammetry, Remote Sensing and Spatial Information Sciences, 41, 221, 2016.

Fonstad, M. A., Dietrich, J. T., Courville, B. C., Jensen, J. L., and Carbonneau, P. E.: Topographic structure from motion: a new development in photogrammetric measurement, Earth Surface Processes and Landforms, 38, 421–430, 2013.

Gindraux, S., Boesch, R., and Farinotti, D.: Accuracy Assessment of Digital Surface Models from Unmanned Aerial Vehicles' Imagery on Glaciers, Remote Sensing, 9, 186, https://doi.org/10.3390/rs9020186, 2017.

Hugenholtz, C., Brown, O., Walker, J., Barchyn, T., Nesbit, P., Kucharczyk, M., and Myshak, S.: Spatial Accuracy of UAV-Derived Orthoimagery and Topography: Comparing Photogrammetric Models Processed with Direct Geo-Referencing and Ground Control Points, GEOMATICA, 70, 21–30, https://doi.org/10.5623/cig2016-102, 2016.

Immerzeel, W. W., Kraaijenbrink, P. D. A., Shea, J. M., Shrestha, A. B., Pellicciotti, F., Bierkens, M. F. P., and de Jong, S. M.: High-resolution monitoring of Himalayan glacier dynamics using unmanned aerial vehicles, Remote Sensing of Environment, 150, 93–103, https://doi.org/10.1016/j.rse.2014.04.025, 2014.

James, M. R. and Robson, S.: Mitigating systematic error in topographic models derived from UAV and ground-based image networks, Earth Surface Processes and Landforms, 39, 1413–1420, https://doi.org/10.1002/esp.3609, 2014.

James, M. R., Robson, S., and Smith, M. W.: 3-D uncertainty-based topographic change detection with structure-from-motion photogrammetry: precision maps for ground control and directly georeferenced surveys, Earth Surface Processes and Landforms, 42, 1769–1788, 2017.

Johnson, K., Nissen, E., Saripalli, S., Arrowsmith, J. R., McGarey, P., Scharer, K., Williams, P., and Blisniuk, K.: Rapid mapping of ultrafine fault zone topography with structure from motion, Geosphere, 10, 969–986, 2014.

Jouvet, G., Weidmann, Y., Seguinot, J., Funk, M., Abe, T., Sakakibara, D., Seddik, H., and Sugiyama, S.: Initiation of a major calving event on the Bowdoin Glacier captured by UAV photogrammetry, The Cryosphere, 11, 911–921, https://doi.org/10.5194/tc-11-911-2017, 2017.

Jouvet, G., Weidmann, Y., Kneib, M., Detert, M., Seguinot, J., Sakakibara, D., and Sugiyama, S.: Short-lived ice speed-up and plume water flow captured by a VTOL UAV give insights into subglacial hydrological system of Bowdoin Glacier, Remote Sensing of Environment, 217, 389–399, 2018.

King, M.: Rigorous GPS data-processing strategies for glaciological applications, Journal of Glaciology, 50, 601–607, 2004.

Kraaijenbrink, P., Meijer, S. W., Shea, J. M., Pellicciotti, F., Jong, S. M. D., and Immerzeel, W. W.: Seasonal surface velocities of a Himalayan glacier derived by automated correlation of unmanned aerial vehicle imagery, Annals of Glaciology, 57, 103–113, https://doi.org/10.3189/2016AoG71A072, 2016.

Leick, A.: GPS satellite surveying, A Wiley–Interscience publication. United States of America, 2004.

McNabb, R., Hock, R., O'Neel, S., Rasmussen, L. A., Ahn, Y., Braun, M., Conway, H., Herreid, S., Joughin, I., Pfeffer, W., et al.: Using surface velocities to calculate ice thickness and bed topography: a case study at Columbia Glacier, Alaska, USA, Journal of Glaciology, 58, 1151–1164, 2012.

Mian, O., Lutes, J., Lipa, G., Hutton, J., Gavelle, E., and Borghini, S.: Direct georeferencing on small unmanned aerial platforms for improved reliability and accuracy of mapping without the need for ground control points, The international archives of photogrammetry, remote sensing and spatial information sciences, 40, 397, 2015.

Minchew, B., Simons, M., Riel, B., and Milillo, P.: Tidally induced variations in vertical and horizontal motion on Rutford Ice Stream, West Antarctica, inferred from remotely sensed observations, Journal of Geophysical Research: Earth Surface, 122, 167–190, 2017.

Morlighem, M., Williams, C. N., Rignot, E., An, L., Arndt, J. E., Bamber, J. L., Catania, G., Chauché, N., Dowdeswell, J. A., Dorschel, B., et al.: BedMachine v3: Complete bed topography and ocean bathymetry mapping of Greenland from multibeam echo sounding combined with mass conservation, Geophysical research letters, 44, 2017.

Mulsow, C., Kenner, R., Bühler, Y., Stoffel, A., and Maas, H.-G.: Subaquatic digital elevation models from UAV-imagery, International Archives of the Photogrammetry, Remote Sensing & Spatial Information Sciences, 42, 2018.

Nesbit, P. R. and Hugenholtz, C. H.: Enhancing UAV–SfM 3D Model Accuracy in High-Relief Landscapes by Incorporating Oblique Images, Remote Sensing, 11, 239, 2019.

Ng, Y. H. and Buchheim, J.: WingtraOne PPK Assessment, White Paper, Wingtra, 2018.

Palmer, S., Shepherd, A., Nienow, P., and Joughin, I.: Seasonal speedup of the Greenland Ice Sheet linked to routing of surface water, Earth and Planetary Science Letters, 302, 423–428, 2011.

Porter, C., Morin, P., Howat, I., Noh, M.-J., Bates, B., Peterman, K., Keesey, S., Schlenk, M., Gardiner, J., Tomko, K., Willis, M., Cloutier, M., Husby, E., Foga, S., Nakamura, H., Platson, M., Wethington, Michael, J., Williamson, C., Bauer, G., Enos, J., Arnold, G., Kramer, W., Becker, P., Doshi, A., D'Souza, C., Cummens, P., Laurier, F., and Bojesen, M.: ArcticDEM, https://doi.org/10.7910/DVN/OHHUKH, https://doi.org/10.7910/DVN/OHHUKH, 2018.

Quincey, D. J., Glasser, N. F., Cook, S. J., and Luckman, A.: Heterogeneity in Karakoram glacier surges, Journal of Geophysical Research: Earth Surface, 120, 1288–1300, 2015.

Rignot, E., Box, J., Burgess, E., and Hanna, E.: Mass balance of the Greenland ice sheet from 1958 to 2007, Geophysical Research Letters, 35, 2008.

Roze, A., Zufferey, J.-C., Beyeler, A., and McClellan, A.: eBee RTK Accuracy Assessment, White Paper, SenseFly, 2014.

Ryan, J. C., Hubbard, A. L., Box, J. E., Todd, J., Christoffersen, P., Carr, J. R., Holt, T. O., and Snooke, N.: UAV photogrammetry and structure from motion to assess calving dynamics at Store Glacier, a large outlet draining the Greenland ice sheet, The Cryosphere, 9, 1–11, 2015.

Ryan, J. C., Hubbard, A., Box, J. E., Brough, S., Cameron, K., Cook, J. M., Cooper, M., Doyle, S. H., Edwards, A., Holt, T., Irvine-Fynn, T., Jones, C., Pitcher, L. H., Rennermalm, A. K., Smith, L. C., Stibal, M., and Snooke, N.: Derivation of High Spatial Resolution Albedo from UAV Digital Imagery: Application over the Greenland Ice Sheet, Frontiers in Earth Science, 5, https://doi.org/10.3389/feart.2017.00040, 2017.

Seier, G., Kellerer-Pirklbauer, A., Wecht, M., Hirschmann, S., Kaufmann, V., Lieb, G. K., and Sulzer, W.: UAS-Based Change Detection of the Glacial and Proglacial Transition Zone at Pasterze Glacier, Austria, Remote Sensing, 9, 549, https://doi.org/10.3390/rs9060549, 2017.

Shahbazi, M., Sohn, G., Théau, J., and Menard, P.: Development and evaluation of a UAV-photogrammetry system for precise 3D environmental modeling, Sensors, 15, 27 493–27 524, 2015.

Strick, R. J., Ashworth, P. J., Sambrook Smith, G. H., Nicholas, A. P., Best, J. L., Lane, S. N., Parsons, D. R., Simpson, C. J., Unsworth, C. A., and Dale, J.: Quantification of bedform dynamics and bedload sediment flux in sandy braided rivers from airborne and satellite imagery, Earth Surface Processes and Landforms, 2018.

Tahar, K.: An evaluation on different number of ground control points in unmanned aerial vehicle photogrammetric block, Int. Arch. Photogramm. Remote Sens. Spat. Inf. Sci, 40, 93–98, 2013.

Taylor, Z. J., Gurka, R., Kopp, G. A., and Liberzon, A.: Long-duration time-resolved PIV to study unsteady aerodynamics, IEEE Transactions on Instrumentation and Measurement, 59, 3262–3269, 2010.

Tedstone, A. J., Nienow, P. W., Gourmelen, N., Dehecq, A., Goldberg, D., and Hanna, E.: Decadal slowdown of a land-terminating sector of the Greenland Ice Sheet despite warming, Nature, 526, 692, 2015.

Todd, J., Christoffersen, P., Zwinger, T., Råback, P., Chauché, N., Benn, D., Luckman, A., Ryan, J., Toberg, N., Slater, D., and Hubbard, A.: A Full-Stokes 3D Calving Model applied to a large Greenlandic Glacier, Journal of Geophysical Research: Earth Surface, https://doi.org/10.1002/2017JF004349, 2018.

Tonkin, T. N. and Midgley, N. G.: Ground-Control Networks for Image Based Surface Reconstruction: An Investigation of Optimum Survey Designs Using UAV Derived Imagery and Structure-from-Motion Photogrammetry, Remote Sensing, 8, 786, https://doi.org/10.3390/rs8090786, 2016.

van der Sluijs, J., Kokelj, S., Fraser, R., Tunnicliffe, J., and Lacelle, D.: Permafrost Terrain Dynamics and Infrastructure Impacts Revealed by UAV Photogrammetry and Thermal Imaging, Remote Sensing, 10, 1734, 2018.

Weidick, A., Williams, R. S., and Ferrigno, J. G.: Satellite image atlas of glaciers of the world: Greenland, 1995.

Westoby, M. J., Brasington, J., Glasser, N. F., Hambrey, M. J., and Reynolds, J.: 'Structure-from-Motion'photogrammetry: A low-cost, effective tool for geoscience applications, Geomorphology, 179, 300–314, 2012.

Wigmore, O. and Mark, B.: Monitoring tropical debris-covered glacier dynamics from high-resolution unmanned aerial vehicle photogrammetry, Cordillera Blanca, Peru, The Cryosphere, 11, 2463–2480, https://doi.org/10.5194/tc-11-2463-2017, 2017.